PHILOSOPHICAL TRANSACTIONS A

royalsocietypublishing.org/journal/rsta

Review

Cite this article: Geneaux R, Marroux HJB, Guggenmos A, Neumark DM, Leone SR. 2019 Transient absorption spectroscopy using high harmonic generation: a review of ultrafast X-ray dynamics in molecules and solids. *Phil. Trans. R. Soc. A* **377**: 20170463.
http://dx.doi.org/10.1098/rsta.2017.0463

Accepted: 27 November 2018

One contribution of 15 to a theme issue 'Measurement of ultrafast electronic and structural dynamics with X-rays'.

Subject Areas:
spectroscopy, solid-state physics, molecular dynamics

Keywords:
ultrafast dynamics, transient absorption, X-rays

Authors for correspondence:
Romain Geneaux
e-mail: rgeneaux@berkeley.edu
Hugo J. B. Marroux
e-mail: hugomarroux@lbl.gov
Stephen R. Leone
e-mail: srl@berkeley.edu

†These authors contributed equally to this study.

THE ROYAL SOCIETY PUBLISHING

Transient absorption spectroscopy using high harmonic generation: a review of ultrafast X-ray dynamics in molecules and solids

Romain Geneaux[1,3,†], Hugo J. B. Marroux[1,3,†], Alexander Guggenmos[1,3], Daniel M. Neumark[1,3] and Stephen R. Leone[1,2,3]

[1]Department of Chemistry, and [2]Department of Physics, University of California, Berkeley 94720, CA, USA
[3]Chemical Sciences Division, Lawrence Berkeley National Laboratory, Berkeley 94720, CA, USA

Attosecond science opened the door to observing nuclear and electronic dynamics in real time and has begun to expand beyond its traditional grounds. Among several spectroscopic techniques, X-ray transient absorption spectroscopy has become key in understanding matter on ultrafast time scales. In this review, we illustrate the capabilities of this unique tool through a number of iconic experiments. We outline how coherent broadband X-ray radiation, emitted in high-harmonic generation, can be used to follow dynamics in increasingly complex systems. Experiments performed in both molecules and solids are discussed at length, on time scales ranging from attoseconds to picoseconds, and in perturbative or strong-field excitation regimes.

This article is part of the theme issue 'Measurement of ultrafast electronic and structural dynamics with X-rays'.

1. Introduction

The knowledge of properties of matter comes hand in hand with our ability to measure it beyond our natural senses. During the past century, our understanding has drastically widened owing to the ability to control light

in numerous ways. A discovery of particular importance is that of a 'new kind of rays' by W.C. Röntgen in 1895 [1], who named them using the commonly used letter for unknowns, X. The discovery of these new-found X-rays earned him the first Nobel Prize in Physics, which opened a new era of research in a great number of scientific areas. X-rays are characterized by very short wavelengths, typically 0.01–10 nm, with enough energy per photon to access transitions from the core levels of atoms. Accessing these transitions, especially with synchrotron radiation, gave chemists and physicists a new tool of X-ray spectroscopy that is now commonly used to study properties of atoms, molecules and solids at equilibrium [2,3], both for fundamental enquiries and applied systems characterization [4,5].

The temporal structure of X-rays emitted from synchrotron sources mirrors that of the electrons used to produce them: typically, a train of 10–100 ps long pulses separated by a few nanoseconds [6]. Synchrotron sources alone are therefore limited in the time resolution they provide, prohibiting the study of many non-equilibrium dynamics. At much longer wavelengths, ultrafast spectroscopy has, on the other hand, allowed for observation of chemical dynamics with time resolutions on the same order as nuclear motion. These advances in the field of physical chemistry were of major importance and have been recognized by the 1999 chemistry Nobel Prize awarded to Ahmed Zewail [7].

In this context, scientists were faced with an interesting prospect: can core-level probing provided by X-rays be combined with the exceptional temporal resolution of femtosecond pulses? This goal has turned into a resounding success, with the availability of complementary ultrafast X-ray sources, such as free-electron lasers [8–11], femtosecond slicing of the electron bunch at synchrotrons [12,13] or high-harmonic generation (HHG) [14–18]. Each of these sources has distinct characteristics; for instance, HHG produces relatively lower photon fluxes but benefits from greater flexibility of implementation. Indeed, extreme ultraviolet (XUV) pulses generated by HHG with femtosecond optical lasers can be produced in most laboratories. Additionally, its properties (spectrum centre frequency, pulse duration, polarization state) can be directly controlled by acting on the driving laser—a more manageable act than manipulating electron bunches by accelerator fields. In turn, HHG revealed to be a fascinating light source with unique properties, perhaps the most important of which is the possibility of generating pulses of attosecond duration. This greatly improved the experiments' time resolution from being on the time scale of nuclear motion, to the fundamental time scale of electron motion.

Initially focused on understanding the process of HHG itself, the field of attosecond science has now transitioned to a wider scope, with HHG sources being used to unravel increasingly complex ultrafast dynamics. As such, several time-resolved spectroscopic techniques were developed, wherein dynamics are typically initiated in the sample by a laser pulse and followed by high-harmonic radiation probing. These techniques differ in the observable that is being tracked: transient absorption spectroscopy follows the absorption of X-rays, while photoelectron spectroscopy measures the electrons that they release, and high-harmonic spectroscopy studies the harmonic radiation emitted by the system. Many excellent reviews on the aforementioned themes already exist; for instance, in the subjects of attosecond science [19–21], free-electron lasers [8], X-ray ultrafast spectroscopy [22,23] as well as an up-to-date overview of X-ray sources in the present theme issue.

In this review, we focus on a rapidly emerging X-ray spectroscopic technique: transient absorption performed with high-harmonic sources. As will be shown, transient absorption is an all-optical technique and does not rely on the emission of photoelectrons or photoions. As such, the time and frequency resolutions are not interdependent through the uncertainty principle, and both can be optimally short and narrow, respectively (attosecond to femtosecond in time and approx. 10 meV in energy). This feature of transient absorption was discussed by Pollard *et al.* [24] in the context of using visible pulses, but directly translates to the techniques described in this review.

The method can be performed using XUV or soft X-ray radiation; for the sake of simplicity, we will indistinguishably refer to the method as X-ray transient absorption spectroscopy (XTAS). After outlining the working principle of X-ray transient absorption, we illustrate how it can be

applied to follow both electronic and structural dynamics using iconic experiments. Despite the impossibility of writing a comprehensive review, we aim to discuss a wide range of dynamics, from attoseconds to picoseconds, in regimes of perturbative or nonlinear excitation, and in various systems; as such, one part focuses on chemical dynamics, while the second addresses processes in condensed matter.

2. Attosecond transient spectroscopy in the gas phase

Transient absorption is a well-developed technique in frequency ranges spanning ultraviolet, visible and mid-infrared. A pump pulse first creates a population in the excited state of the system. The population is allowed to evolve freely during a defined duration, at which a probe pulse—often broadband—induces transitions to other excited states. By frequency-resolving the absorption of the probe pulse across its spectrum, signatures of the current state of the system can be identified. Spectral features can be linked for instance to chemical functional groups or evolution of ground- and excited-state populations. In practice, the probe spectrum is measured at each time step, with (I_{on}) and without (I_{off}) the pump pulse, and the measured quantity is the change in absorption in optical density, $\Delta OD = -\log_{10}(I_{on}/I_{off})$. We note that in addition to transferring population, a strong pump pulse may also modify the molecular potential, for example through bond softening [25] or creation of light-induced vibrational states [26].

The difficulty of this technique in the visible to ultraviolet frequency range comes when spectral features from different excited states or photoproducts overlap, due to either small shifts or/and broadband transitions. This often prevents a simple assignment of measurements to chemically relevant information. This hindrance can be overcome by using much shorter wavelengths; indeed, the core-levels of different elements have very distant ionization energies. As is known from synchrotron-based studies, these so-called absorption edges lie in the XUV and X-ray regions, and their spectrum is remarkably sensitive to the electronic environment and molecular structure surrounding the element. As such, performing transient absorption with a XUV/X-ray probe yields more information than in the visible, for instance on the oxidation state, coordination or bond nature [27,28].

Therefore, XTAS relies on the generation of short pulses of XUV light, synchronized with a visible pump pulse. This is naturally realized in HHG, where femtosecond visible pulses are upconverted into the XUV. At each half-period of the driving field, an attosecond burst of light is emitted, as explained by the simple three-step model [29,30]. For a relatively long driver, these bursts interfere to create a series of discrete harmonics in the spectral domain and an attosecond pulse train (APT) in the time domain. By contrast, if the driver duration is kept close to the optical cycle duration, isolated attosecond pulses (IAPs) with broadband continuum spectra are emitted. As we will see, both types of radiation are used in XTAS, providing time resolutions in the range of tens of femtoseconds and hundreds of attoseconds, respectively.

In the first part of this review article, the several ways in which XTAS can be used to probe gas-phase chemical dynamics are presented. First, we present femtosecond-resolved experiments and showcase the information yielded by using broadband XUV radiation as a probe. Then, we focus on experiments investigating strong-field phenomena probed with IAPs, adding unparalleled temporal resolution. Finally, experiments in which the pulse order is reversed are highlighted: here the attosecond pulse is used first to populate excited states located in the XUV and a subsequent near infrared (NIR) pulse probes their dynamics at a later time.

(a) Extreme ultraviolet probing of femtosecond chemical dynamics

The ground-state dynamics of molecules is now well captured by theory in the case of separable nuclear and electronic motions, that is in the adiabatic picture of the Born–Oppenheimer approximation [31]. Nevertheless, excited states dynamics can lead to fast nuclear motion so that the separation of nuclear and electronic degrees of freedom does not hold and non-adiabatic dynamics occurs. Models have been developed in an effort to described the dynamics in such

cases [32] but in order to further understand these important processes, experimentalists need to develop techniques capable of measuring dynamics with increasingly precise time resolution, combined with new features such as element specificity, electronic character sensitive detection, oxidation number sensitivity or electronic spin sensitivity. With these goals in mind, XTAS was developed as a new tool to collect novel information on molecular dynamics by using a broadband XUV probe.

In the first series of experiments presented, HHG is typically driven by 20–40 fs, VIS–IR pulses producing a spectrum of odd discrete harmonics. The covered spectral range extends from ≈14 to 150 eV depending on the generating gas used. In some of these experiments, the spectral coverage is further increased by adding the second harmonic of the driving field, leading to a symmetry-breaking in HHG and to the generation of even harmonics [33]. In the temporal domain, the generated radiation consists of a train of attosecond pulses whose overall duration is similar to the driving field duration. This type of XUV spectrum is capable of covering multiple absorption edges of metal centres or halide substituents. In the associated core-level transitions, the wave function of the initial state is localized on a single atom, therefore allowing for observation of the dynamics from the 'point of view' of this element, contrarily to valence transitions, which often involve states with wave functions delocalized over several atoms. This, combined with femtosecond pulse durations, allows for element-specific probing of ultrafast dynamics.

A notable example is that of the photodissociation dynamics of bromoiodomethane (CH_2IBr) [34]: when excited by 266 nm pulses, molecules dissociate via two accessible channels: either C-I bond breaking after a $n(\mathrm{I}) \rightarrow \sigma^*(\mathrm{I})$ transition or C-Br bond breaking after a $n(\mathrm{Br}) \rightarrow \sigma^*(\mathrm{Br})$ transition, as indicated in figure 1*a*. Both dissociation channels are fast and require the use of an accordingly short pulse. Attar *et al*. [34] studied this process using XTAS, which not only provides the necessary time resolution, but a broad probing bandwidth. Thus, the dissociation can be followed simultaneously from the point of view of the bromine and iodine atoms, whose absorption edges lie at 67 and 51 eV, respectively. Figure 1*a* shows the transient spectra at both edges averaged for time delays between 0.5 and 1 ps. By observing the growth of the transitions in the atomic fragment, they were able to follow the dissociation along both the C-I and the C-Br bonds simultaneously and to determine the associated time constants of 45 ± 12 and 114 ± 17 fs, respectively.

Even in the presence of a single element, XTAS is able to separate competing pathways. For instance, dissociation products originating from different channels might be in different electronic states. Owing to its sensitivity to the spin–orbit coupling of the probed state, the core-level absorption will vary between dissociation products. In a different study, Attar *et al.* investigated the photodissociation of methyliodide (CH_3I) after valence excitation by 266 nm photons [35]. At this excitation energy, an electronic transition from the non-bonding orbital of iodine to an anti-bonding orbital with $^3Q_0$ character is known to dominate the dynamics and leads to photodissociation as indicated by the potential energy curve shown in figure 1*b*. Owing to the large spin–orbit coupling of the iodine atom, intersystem crossing to the $^1Q_1$ state can be accessed via a conical intersection located near the Franck–Condon region. The two photodissociation channels lead to a methyl fragment with the iodine atom in either its ground state originating from the $^1Q_1$ state, or spin–orbit excited state originating from the $^3Q_0$ state. These two fragments have different core-to-valence transition energies so the growth of dissociation products originating from the $^1Q_1$ to $^3Q_0$ states can be followed simultaneously and the branching ratio can be determined.

In addition to these end products, Attar *et al*. identified features in the early times of the dissociation dynamics. The transient spectrum at 50 fs is shown in blue in figure 1*b* and shows two additional features (labelled transient features A and B) which are attributed to propagation of the wave packet in a transition state region (shaded area in the potential energy curves) located between the Franck–Condon region and the dissociation limit. Bhattacherjee *et al*. [38] also observed similar features in allyl iodide. The observed transition state feature reported by Attar *et al*. lives for 90 fs, making it one of the shortest transition state reported using XTAS in a molecular system. Drescher *et al*. [39] conducted a similar study of methyl iodide using XTAS but

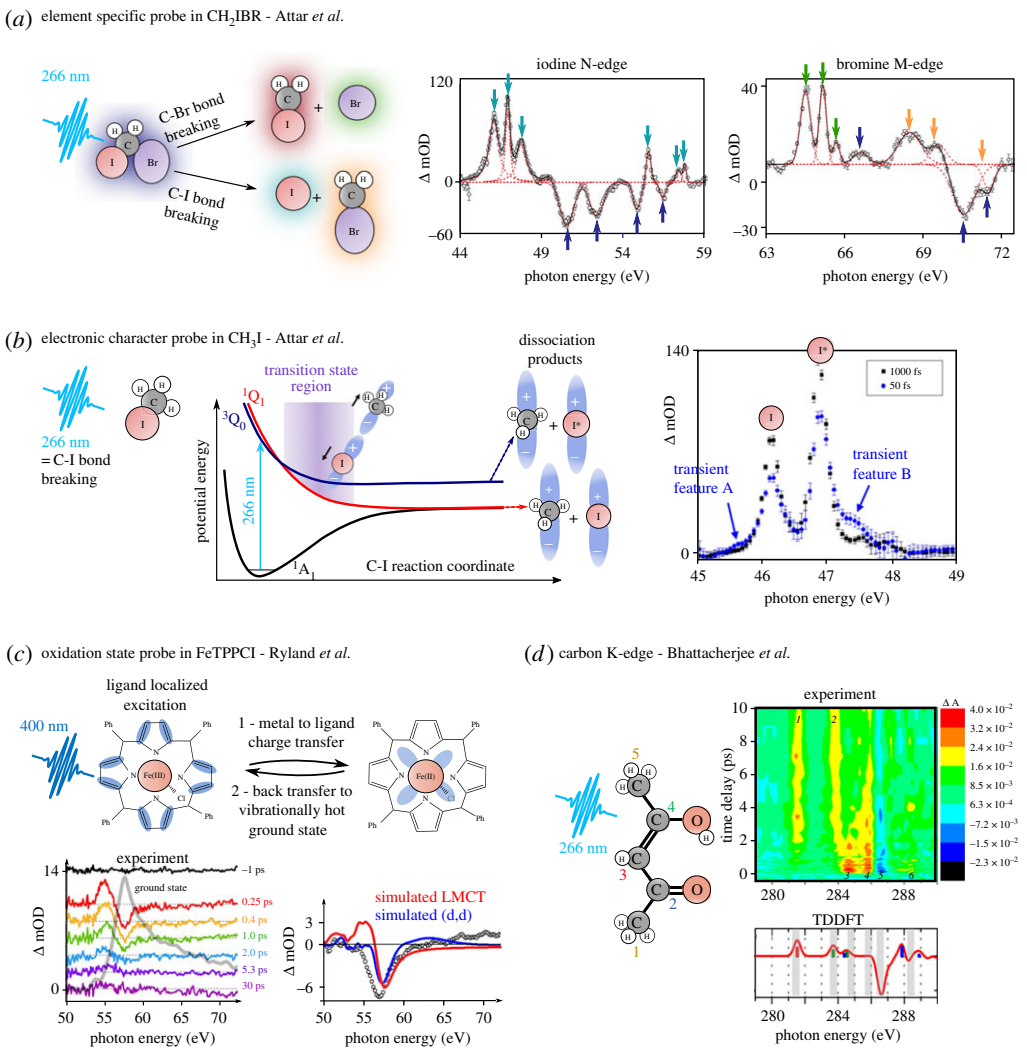

Figure 1. Broadband XUV probing of gas-phase chemical dynamics. (*a*) Element-specific core-level probing of the photodissociation dynamics of CH_2IBr using XTAS at the iodine and bromide edges. Adapted with permission from [34]. The pump pulse promotes a valence transition. The XTAS spectra averaged between 0.5 and 1 ps are shown at the two atomic edges. (*b*) Probing the electronic character of iodine fragments following the dissociation of CH_3I after 266 nm excitation. Adapted with permission from [35]. The potential energy curves along the C-I distance are shown for ground and excited states with the transition state regions in shaded area and the spin–orbit specific transitions indicated. Two transient spectra at the iodine edge at 50 and 1000 fs are shown to illustrate the new features of the transition state. (*c*) Following the time evolution of the oxidation number of a haem-type complex following 400 nm excitation. Adapted with permission from [36]. The XTAS spectra at the iron M-edge are shown for various time delays along with the simulated spectrum for the LMCT and (d,d) states. (*d*) Probing intersystem crossing dynamics of acetylacetone after 266 mn excitation using carbon K-edge XTAS. Adapted with permission from [37]. The molecular structure is shown with the carbon labelling colour coding corresponding to the stick bar plot shown in the transient spectrum calculated for the triplet states by TDDFT.

due to a poorer time resolution only observed a time-dependent shift in the XUV transition rather than distinct features.

Element-specific information is also advantageous in large molecules such as metal complexes to focus the investigation on only a selected part of the system. Transient absorption experiments using a visible probe on such complexes often display broadband overlapping features of

transitions localized on the ligands and the metal centre, complicating the interpretation of the spectrum. XTAS presents the advantage of following the excited state dynamics from the point of view of the metal centre only. Moreover, XTAS at the M- and L-edges of metals offers a sensitive probe to the oxidation number, delivering key information on the evolution of the chemical reactivity of the complex. Using HHG-based transient absorption, Ryland *et al*. were able to follow the time evolution of iron(III) tetraphenyl porphyrin chloride, a haem precursor, after excitation of a $\pi \rightarrow \pi^*$ transition localized on the complex's ligand [36]. This excited state then evolves to a ligand to metal charge transfer state (LMCT) changing the oxidation number of the complex's metal centre as illustrated in figure 1*c*. By following the time evolution of the absorption spectrum of the iron atom M-edge located between 50 and 65 eV (3p → 3d transition), Ryland *et al*. were able to follow the dynamics of transfer of the wave packet from the ligand localized state to the metal centre. After formation of this LMCT state, two decay mechanisms have been contemplated in the literature, either a direct decay to a vibrationally hot ground state formed by back electron transfer to the ligand, or evolution to a metal centre excited state, the (d,d) excited states. The previously published visible transient absorption spectrum displays a congested spectrum for which disentangling between the two decay mechanisms is not direct [40]. On the other hand, in XTAS the simulated spectrum of the (d,d) state shows two clear features, namely a ground-state bleach at 57.5 eV and a positive feature extending from 60 to 65 eV as shown in figure 1*c*. At no time in the XTAS spectrum is a broad positive feature seen, excluding the (d,d) state as taking part in the decay mechanism of the haem precursor. This work exemplifies the sensitivity of XUV transient absorption on the partial charge of atoms in a large molecular system. This approach can be extended to different systems deposited on thin films, where XUV absorption spectra have shown sensitivity not only to oxidation states of metal centres but also to their spin states and ligand field variations, making XTAS a unique tool to study inorganic compound photoreactivity [41].

We have so far presented experiments where the transition used to probe the system originates from core-levels of halogens or transition metals. Indeed, they consist of the main elements accessible with harmonic spectra up to 150 eV. This unfortunately limits the generality of the technique, and in particular it prevents the study of biologically relevant systems for which most of the important atoms have their core-excitations located above 150 eV. Driven by this prospect, the attosecond community made a remarkable effort in pushing the available photon energy. In turn, recently developed sources have reached the so-called water-window range, which extends from the carbon K-edge at 284 eV to the oxygen K-edge, and even beyond, up to 1.56 keV [42]. Underlying this progress are new drivers for HHG with longer wavelengths.

Despite the low photon flux at those energies, these sources were used to conduct transient absorption experiments; as first shown by Attar *et al*. [43] and Pertot *et al*. [44], respectively, to study the ring-opening reaction of cyclohexadiene and the dissociations of SF_6 and CF_4 following strong-field ionization. In a subsequent study, Bhattacherjee *et al*. showed the sensitivity of carbon K-edge transient absorption on electronic configuration changes in studying the time evolution of acetylacetone after 266 nm excitation [37]. In their transient absorption traces, the authors observed an isolated positive feature at 281.4 eV growing in on a sub-2 ps time scale, labelled feature 1 in figure 1*d*. Using time-dependent density functional theory, the authors assigned this feature to the lowest triplet state populated following internal conversion and intersystem crossing. From their calculations, they also show that this transition corresponds to a core-to-valence transition localized mainly on carbon 3 (see the labelling in figure 1*d*). Other transient peaks can also be associated with specific carbons as shown by the colour coded stick spectrum.

(b) Isolated attosecond pulses and strong-field dynamics

It is valuable to consider the time resolution of the experiments. Experiments presented so far are performed in the perturbative regime where field-driven effects are negligible and the time resolution is determined by the cross correlation between pump and probe pulses, determined by the pulse time envelopes.

When the electric field of light is on the order of the atomic Coulomb potential (approx. $5 \times 10^{11}\,\mathrm{V\,m^{-1}}$), the response of the system can no longer be expressed as a perturbative expansion of the permittivity. In turn, non-perturbative strong-field dynamics takes place and time evolutions on the time scale of the field oscillation can been seen. To capture these field-driven dynamics, it becomes necessary to reduce the probe duration by producing isolated XUV attosecond pulses rather than the previously mentioned attosecond pulse trains. Several techniques are now available to isolate a single attosecond pulse and are discussed in several review articles [17,45].

One of the long-standing goals of attosecond spectroscopy is to observe pure electronic dynamics. Using a few-cycle visible pulse, Goulielmakis *et al*. [46] were able to create superpositions of electronic states in ionized krypton atoms. The time evolution of the electronic wave packet was followed by transient absorption using an isolated XUV pulse centred around the $4p \rightarrow 3d$ core-to-valence transition of the cation. Strong oscillations are seen in the absorption features at a frequency of 6.3 fs owing to the wave packet created between the two spin–orbit states of the krypton cation (split by 0.67 eV). Knowing the phase and amplitude of this superposition, the authors were able to reconstruct the time evolution of the electronic wave packet with sub-femtosecond resolution (shown in figure 2*a*).

Recently, Kobayashi *et al.* conducted a similar experiment [47] in xenon where single, double and triple-ionization products were produced. Here, the authors not only observed oscillations in time traces due to the beating of the electronic wave packet of the doubly ionized atom, but they also determined that the formation of doubly ionized products was delayed compared with singly ionized ones by delays ranging from 650 to 850 attoseconds, depending on the final state considered. The kinetics traces of formation of Xe^{+} and Xe^{2+} are shown in figure 2*b* in black and yellow, respectively. These experimental time delays do not match with time delays obtained from an uncorrelated electron-emission model, suggesting that electron correlation might play a role in the di-cation formation.

One of the issues with using strong-field ionization as a pump is the lack of selectivity regarding the distribution of eigenstate populations it creates. Wei *et al*. used a short train of attosecond pulses as a probe centred around the $4d \rightarrow 5p$ core-to valence transition of iodine to study strong-field dynamics in methyl iodide [48]. In this region of the spectrum, molecular cationic and neutral iodine transitions are spectrally separated so dynamics of the two eigenstates can be resolved independently. By observing the energy shift as a function of time in the transition associated with ground-state neutral methyl iodide at 50.7 eV, they were able to identify two excitation mechanisms, namely bond softening and R-selective depletion. Figure 2*c* shows two schematic potential energy curves illustrating the two mechanisms. In R-selective depletion, the intense pump ionizes the neutral molecule with various efficiencies depending on the C-I internuclear distance (R). This results in an unequally distributed wave packet along the C-I coordinate (in green); the original wave packet is shown in yellow for comparison purposes. Initial motion of this wave packet will be towards shorter C-I distances to retrieve an equilibrium distribution. In bond softening, a vibrational wave packet is created by modification of the Morse-like potential curvature [51] by the intense field as shown in figure 2*c*. This results in a wave packet initially moving towards longer C-I distances. The two so-created wave packets will evolve at similar C-I stretching frequencies, but with different phases as illustrated by the schematics showing the time evolution of $\langle R \rangle$. Owing to the highly repulsive nature of the core-hole excited state probed by the XUV, changes in the internuclear distance of C-I is reflected by a change in XUV absorption frequency. This allows the separate observation of the two processes despite the lack of selectivity at the pump step. Figure 2*c* shows the time evolution of the maximum of the central transient absorption feature of the neutral molecule. The time evolution was fitted by the authors to two oscillatory components, with phases of $(-0.49 \pm 0.05)\,\pi$ and $(-0.09 \pm 0.12)\,\pi$ associated, respectively, with the bond softening and R-selective depletion mechanisms.

Strong-field interaction can be used to manipulate electronic dynamics of excited states located in the XUV and populated by the weak attosecond pulse. In the following experiments, the broadband attosecond pulses are used to initiate dynamics, so the pulse ordering is reversed

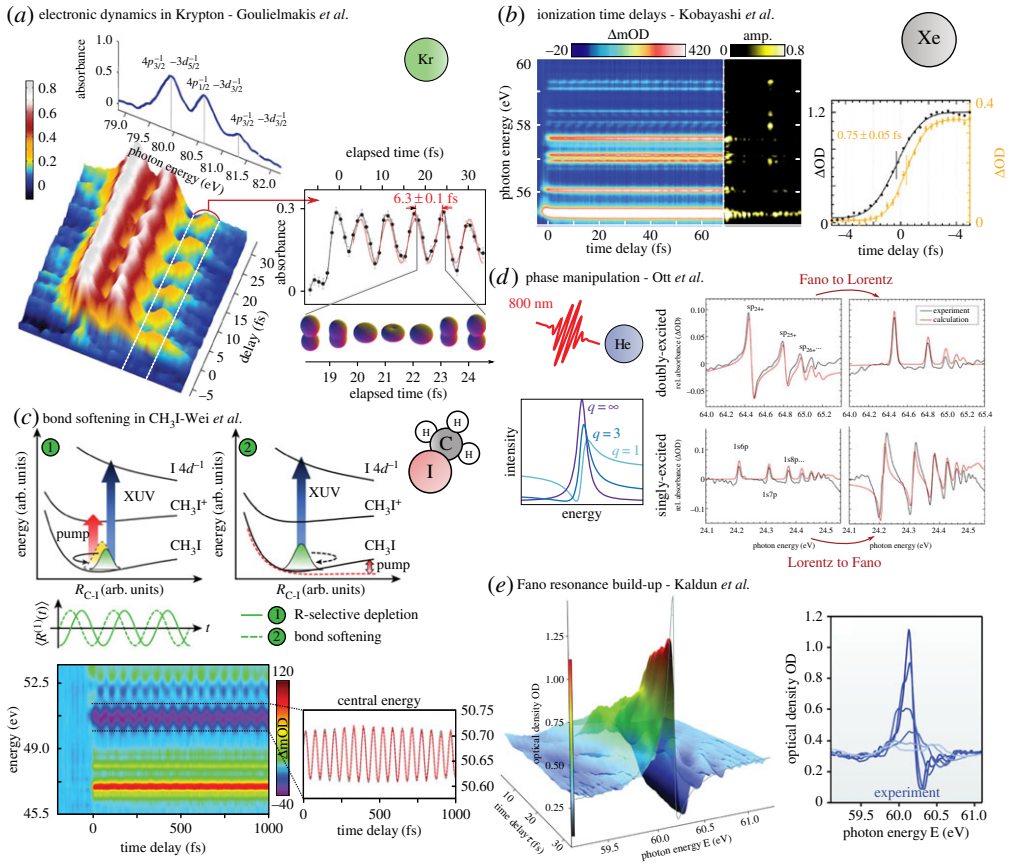

Figure 2. Gas-phase strong-field dynamics. (*a*) Electronic wavepacket reconstruction, adapted with permission from [46]. The time evolution of the XTAS spectrum is shown with corresponding transitions. From the oscillations in the time trace, the wavepacket time evolution is reconstructed. (*b*) Ionization time delay in xenon, adapted with permission from [47]. XTAS spectra following ionization of xenon are shown. Kinetics traces of features corresponding to Xe^{+} and Xe^{2+} formation are shown in black and yellow, respectively. (*c*) Differentiating strong-field excitation mechanisms in CH_3I. Adapted with permission from [48] Potential energy curves along the C-I distance are shown with the two pumping mechanisms involved. The expected time evolution of the wave packet position ($\langle R^{(1)}(t)\rangle$) for the R-selective depletion and bond softening mechanism is shown in solid and dashed line, respectively. The XTAS spectra as a function of time are shown along with the time evolution of the central energy of the ground-state bleach signal. (*d*) Manipulating dipole function, adapted with permission from [49]. A few Fano absorption lineshapes for different values of the *q* parameter are shown. The absorption lineshape of two Rydberg series of He, display Lorentz and Fano lineshapes for singly and doubly excited states, respectively. These lineshapes are transformed into each other under the influence of the NIR field. (*e*) Fano resonance build-up. Adapted with permission from [50]. By changing the arrival time of the strong laser field, the emergence of a Fano line shape, due to the autoionization process, is observed.

compared to previously described XTAS experiments. Following the linear absorption of the XUV pulses, a macroscopic polarization is created across the sample oscillating at the resonant frequencies. Dephasing times of XUV resonances in the gas phase are typically limited by the excited state lifetime, because processes such as Auger decay or autoionization typically take place before a collision occurs. The resulting free induction decay (FID) emits an electromagnetic field (signal field) that interferes with the incident, non-absorbed field, defining the absorption lineshape. This detection scheme, also common to transient absorption, is referred to as self-heterodyned detection [52,53]. This phase sensitive detection leads to the observation of symmetric Lorentzian lineshapes. In autoionizing excited states, coupling of the resonance with the ionization continuum induces a phase shift in the FID, shifting the absorption profile from

a Lorentzian to an asymmetric Fano lineshape. Fano lineshapes arise whenever phase shifts are induced in the FID, they are therefore not limited to autoionizing states, and they have been observed in the Mid-IR, e.g. by coupling a carbonyl stretch around 6 µm with a plasmonic resonance [54].

Fano profiles are described through q, the Fano parameter, which measures the ratio of the resonant to the direct scattering amplitude. Different lineshapes obtained for various values of q are shown in figure 2. By applying a strong-field-induced ponderomotive shift on a resonance, Ott *et al*. [49] were able to manipulate q and therefore change the lineshapes. Figure 2*d* shows absorption lineshapes of singly and doubly excited sates of He. The field-free lineshape of singly excited states around 24–24.5 eV shows a Lorentzian lineshape, because the resonance is located below the first ionization threshold while doubly excited state lineshapes at 64–65.4 eV show Fano lineshapes due to coupling with the continuum. Lineshape modifications are seen in the second row of figure 2*d* where the lineshapes are tuned from Fano to Lorentzian at 64 eV and from Lorentzian to Fano at 24 eV.

This experiment shows that the nonlinear dipole function contains a wealth of information on the system's time evolution. The same group used a similar formalism to observe the build-up of the Fano profile in the time domain [50]. By using an intense field to interrupt the FID at different time delays by ionizing the medium, they were able to see the evolution of the absorption profile from a Lorentzian like profile to a Fano profile as illustrated in figure 2*e*. The time evolution of the lineshape gives direct time-resolved information on the coupling between the resonance and the continuum. The same build up was observed in electron interferometry measurements [55].

(c) N wave mixing spectroscopy

Observation of the macroscopic polarization created by attosecond pulses allows for analogies with spectroscopies typically reserved to the mid-IR and visible part of the electromagnetic spectrum [56]. In these spectral ranges, these techniques add remarkable capabilities, such as spatial resolution, correlation spectroscopy or surface sensitivity, which can be combined with the advantages of XUV/X-ray radiation, namely, element specificity and attosecond resolution.

One such technique is four wave mixing (4WM) spectroscopy, which has now been successfully performed in the XUV in atomic [57–60] and molecular systems [61] by combining XUV pulses with few-cycle NIR pulses. In pioneering work, Warrick *et al*. used 4WM field emission to probe the energy landscape of the excited states of N_2 molecules located at 14 eV [62]. In this part of the spectrum, N_2 shows vibronic progressions in the bright $\boldsymbol{b}'^1\Sigma_u^+$ state. One NIR photon energy below this state, the dark $\boldsymbol{a}''^1\Sigma_g^+$ is accessible, which has a double well structure along the internuclear distance as shown in figure 3.

Using the experimental geometry shown in figure 3*a* where two NIR and one XUV beam are incident on the sample, 4WM field emission is spatially separated from incident radiation and displaced on the CCD camera after being dispersed. Figure 3*a* shows the camera image obtained when all pulses are coincident in time, with the vertical axis converted into emission angles. Centred around 0 mrad on the angular axis, the transmitted XUV pulse spectrum is shown with discrete N_2 absorption lines imprinted by the bright $\boldsymbol{b}'^1\Sigma_u^+$ state. The phase matching condition for the 4WM emission is shown in figure 3*a*. By manipulating the time delay between the three pulses, Warrick *et al*. were able to probe the time evolution of wave packets created either in the inner or the outer well of the $\boldsymbol{a}''^1\Sigma_g^+$ state.

In the first time sequence used, the XUV pulse is synchronized with an NIR pulse, which creates a wave packet in the inner well part of the dark state (in green) via a coincident two photon transition. After a time delay, the second NIR couples the wave packet back to the $\boldsymbol{b}'^1\Sigma_u^+$, which leads to the 4 WM XUV emission. The time evolution of the emission features is shown and there are oscillations due to quantum beat interferences due to the different quantum phases acquired between vibrational states composing the wave packet. Fourier transformation of the time traces shows peaks at emission frequencies and along a line at 0.26 eV, the vibrational frequency of the $\boldsymbol{a}''^1\Sigma_g^+$ inner well. By delaying the first NIR pulse and the XUV by half the vibrational period

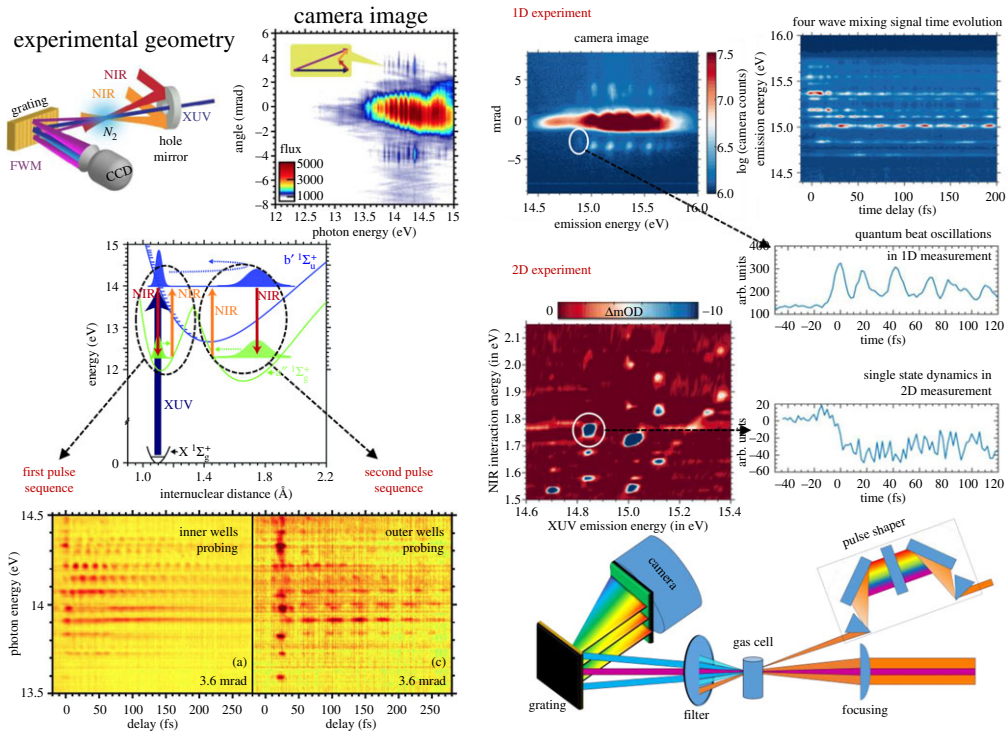

Figure 3. XUV initiated four wave mixing experiments. (*a*) Wavepacket manipulation in N_2 [62]. The experiment geometry is shown with the two NIR beams in red and orange, the incident XUV APT in blue and the resulting 4WM emission in purple. The camera image where the vertical axis is the emission angle is shown. At 0 mrad, we can see the spectrum of the transmitted XUV beam and off-axis, at 4 mrad, the 4WM emission lines. The potential energy curves are reported below with the two coupling schemes allowing for probing of the inner or outer well potential of the $a''^1\Sigma_g^+$ state. The experimental time traces of the 4WM signal, when probing either the inner or outer well, are shown below. (*b*) Two-dimensional spectroscopy at XUV energies [63]. The camera image and time evolution of the one-dimensional measurement are shown along with the state labelling. A pulse shaper is added in one NIR beam of the experiment to collect the two-dimensional spectrum shown. The time traces show the suppression of quantum beats in the two-dimensional spectrum compared to the one-dimensional 4WM time evolution, granting access to the dynamics of a single state of the system.

of the bright state, the dark state wave packet is created in the outer well of $\boldsymbol{a}''$ as illustrated in the energy diagram. The time evolution of this wave packet was then probed by the second NIR pulse, which leads to emission at the same $\boldsymbol{b}'^1\Sigma_u^+$ lines. The time evolution is shown in figure 3*a* and displays oscillations in $\boldsymbol{a}''$ but at lower frequencies than in the previous time trace. The Fourier transform confirms that beats are now observed at 0.10 eV, corresponding to the vibrational frequency of the outer well in the $\boldsymbol{a}''^1\Sigma_g^+$ state.

In this experiment, the number and the energy of the light–matter interactions is well defined, because they are conducted in an intensity regime where the perturbative expansion of the permittivity is a valid approximation. In that regime, the field free atoms or molecular eigenstates can be investigated, but 4WM spectroscopy as presented in the previous experiment does not always report on the time evolution of one or just a few eigenstates at the same time. This can be explained when considering the origin of the quantum beat oscillations. The quantum beats arise from the interferences of two signal fields emitting at the same XUV frequency, but where the populated states during the time delay are different. The beating frequency is the energy difference between the excited states, which can often be coincident for multiple pairs of levels.

Single-state dynamics can be retrieved by again using a technique widely used in the visible and mid-IR. Marroux *et al*. developed a multidimensional spectroscopy in the XUV that provides frequency resolution on the NIR interaction energy while preserving the experiment time resolution [63]. Figure 3*b* shows the usual, one-dimensional transient absorption experiment: the investigated states, the Argon Rydberg series located between 14.5 and 15.8 eV, lead to off-axis 4WM emissions on the camera image and corresponding quantum beat oscillations are seen in the time trace. To transform this experiment into a multidimensional experiment, a pulse shaper is introduced into one of the NIR arms. The pulse shaper applies a narrowband amplitude and phase modulation in one NIR pulse, which is delayed from the two coincident pulses as shown in figure 3*b*. The shaped NIR pulse probes the argon atoms when the wave packet is composed of 4*p* dark states. The two-dimensional spectrum is constructed by recording the 4WM spectrum as a function of the central frequency of the narrowband modulation applied by the shaper, effectively turning off the contribution at this frequency. The obtained spectrum is shown in figure 3*b*, which correlates NIR resonant frequencies and XUV emission. To illustrate the capacity for retrieving eigenstate dynamics, time traces of the one- and two-dimensional experiments are compared. The two-dimensional experimental feature shows a constant time evolution after time zero corresponding to the time evolution of the state, while the one-dimensional experiment shows the previously mentioned quantum beats arising from the interferences of the fields.

On systems where multiple excited states are accessible by the XUV pulse, and each state shows a fast decaying mechanism, two-dimensional spectroscopy is a unique tool capable of probing the dynamics of each of these eigenstates separately, with few femtosecond time-resolution. We can foresee that this technique will become important in probing condensed phase dynamics where homogeneous and inhomogeneous broadening come into play. Multidimensional spectroscopy based on core-level excitation has the potential for capturing these ensemble-resolved effects from the point-of-view of a single element.

3. Attosecond transient spectroscopy of condensed matter

The preceding section highlighted many breakthroughs in gas-phase spectroscopy facilitated by HHG-based transient absorption spectroscopy. The capabilities of this technique—broadband probing, element-specificity and atto- to femtosecond temporal resolution—can advantageously be used to put condensed matter under scrutiny. Here we present several experiments using this technique and discuss what fundamental scientific questions they can answer. We will finally provide a perspective on how this field may develop to give novel insight, not only in test systems, but also in materials relevant to a broader condensed matter community.

The behaviour of an electron in the periodic lattice potential has been an essential question of solid-state physics, from the early works of Drude [64], Sommerfeld & Bethe [65] and Bloch [66], continuing until today. Experimentally, this is investigated by measuring the response of the system to a stimulation, like electromagnetic radiation or heat. The induced change is explained through a response function such as the dielectric function or heat capacity. Throughout the years, various types of probes identified the numerous effects governing electronic dynamics, such as lattice vibrations, electronic correlations or magnetic effects [67]. Along with this understanding came the possibility of driving these dynamics not only far away from their equilibrium but with stimulations strong enough to redefine the eigenstates of the system. For instance, intense static electric fields can be used to distort the band structure of the material enough to alter its properties; Zener tunnelling [68,69], Wannier–Stark localization [70,71] or the Franz–Keldysh effect [72] are some examples.

Short pulses of X-rays, which allow access to both structural and electronic effects, are a remarkable probe of solid-state properties. When a solid is irradiated by a light pulse, the medium's complex refractive index is transiently modified. Underlying this change is the motion of the medium's constituent electrons as well as that of the lattice. As we have seen in the gas phase, electrons can react on attosecond time scales. As such, XTAS is one of the only tools able to fully track this response. Hereafter, we distinguish two types of XTAS experiments, which aim to

answer different questions. First, we present experiments focused on the almost instantaneous nonlinear response of electrons to a strong driving pulse. This work reveals ultrafast, non-equilibrium dynamics and aims to answer a crucial question: how fast can a material's properties be modulated? Second, we describe another body of experiments that study the system's response to a change in its equilibrium population distribution. Here, XTAS answers different questions: in what way and how fast is the deposited energy redistributed? What are the mechanisms at play? In turn, can systems be engineered to control these redistribution processes?

(a) Ultrafast nonlinear processes in materials

Nonlinear light-matter processes are ubiquitous in modern optics and have enabled scientists to control matter with light—and vice versa. Among many examples are nonlinear crystals, in which various wavelengths can be generated and manipulated to form Kerr lenses, which are widely used to passively mode-lock femtosecond oscillators. These processes are driven by intense femtosecond pump pulses, typically at visible or near-infrared wavelengths. In the nonlinear interaction, the underlying electronic motion responds at the scale of the optical cycle and can only be probed by an accordingly shorter probe pulse, such as an IAP.

These XUV pulses probe core-to-valence band (VB) or core-to-conduction band (CB) transitions typically with bandwidths on the order of $\Delta E \sim 10\,\mathrm{eV}$. The resulting macroscopic polarization dephases within $\hbar/\Delta E \sim 100$ as, setting the time resolution of the pump–probe experiments. Consequently, XTAS presents us with a way to 'zoom in' on the electronic states in real-time.

We have chosen to highlight five results from the literature that all study sub-cycle electronic dynamics, but in materials of very different bandgaps. Together they illustrate how, depending on the excitation regime, various nonlinear phenomena arise. They are presented side to side in figure 4.

Nonlinear effects are best observed in transparent materials: if the linear absorption coefficient is low in the VIS-IR, the field strength of the pump pulse can be increased without substantial carrier excitation, heating or reaching the breakdown of the material. Accordingly, the first of these experiments by Schultze *et al*. [73] was performed in silicon dioxide (SiO_2), a dielectric material of 9 eV direct bandgap. After being pumped by a visibleNIR (VIS–NIR) pulse of less than 4 fs, the material is probed by a 72 as IAP. Its energy is chosen to match the Si 2p states (equivalently, the $L_{2,3}$-edge, lying at approx. 99 eV), so that transitions from these core-levels to the VB/CB are possible. Experimentally, as a general rule, the thickness of the sample must be kept on the order of the attenuation length (82 nm for SiO_2 at 105 eV) in order to measure its XUV absorption. This mandates the use of thin films, either free-standing or deposited on a thin membrane (typically Si_3N_4). Here, a 125 nm free-standing film is used.

Owing to the wide bandgap of SiO_2, the VIS-IR pulse (1.5 eV central energy) is unable to promote real carriers from the valence to the conduction band. Consequently, the absorption observed in [73] does not change as long as the pump and probe pulse do not overlap in time. By contrast, the XUV absorption changes drastically during the pump–probe overlap (figure 4*a*). Its amplitude, as well as the position of the absorption peak, oscillates at twice the driving laser frequency. This suggests that the mechanism at play is directly linked to the driving electric field, and it has been interpreted as a manifestation of Wannier–Stark localization [71]. In this phenomenon, a strong static electric field creates highly localized electronic states at lattice sites. In turn, all the bands of the material shift as the field strength increases. For a strong enough field, the shifted bands of neighbouring lattice sites can cross, leading to a mixing of valence and conduction bands. When projected back to the field-free band structure, this looks like a transient electron (hole) population in the CB (VB), therefore called virtual carriers. As shown by the experiment of Schultze *et al*., this effect is fully reversible, providing a way towards controlling the material's dielectric function at twice the optical frequency; that is, at the petahertz level. This constitutes a significant progress compared to present-day electronics, which operate at terahertz frequency, at most [65]. We note that a recent work [78] revisited this experiment and proposed

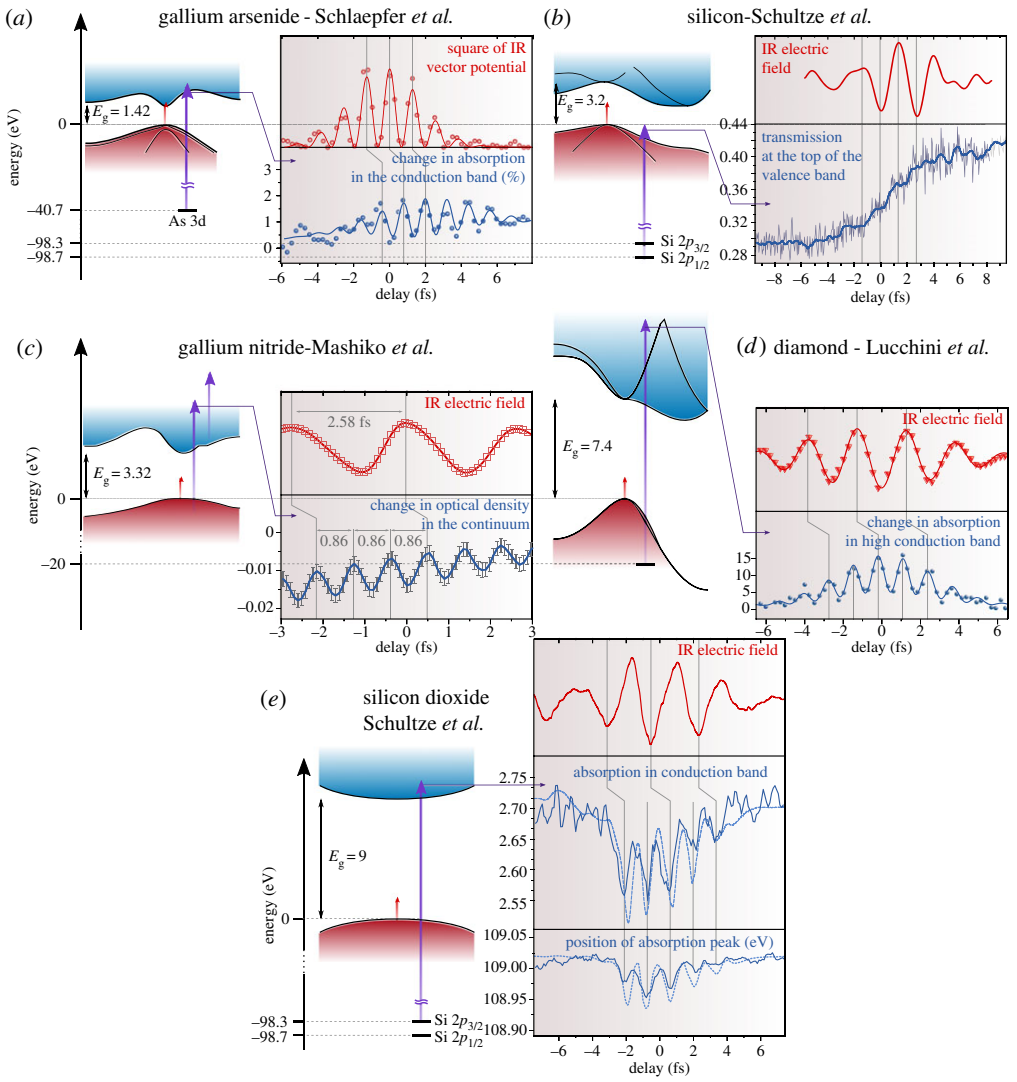

Figure 4. Attosecond spectroscopy of nonlinear processes in solids. Summary of the five experiments presented. For each, the band structure of the material is sketched on the left, with the VB in red, the CB in blue, their bandgap energy E_g (expressed in eV), the VIS-IR pump pulse (red arrow) and the isolated attosecond probe pulse (purple arrow). On the right is shown the temporal profile of the VIS-IR measured by streaking (red line), as well as the transient absorption measurement (blue line), expressed either in absorption change, transmission or optical density. Grey lines guide the eye to visualize the periodicity of the transients compared to the VIS-IR frequency. (*a*) Wannier–Stark localization in Silicon Dioxide, adapted with permission from [73]; (*b*) inter-band tunnelling from the VB to the CB in Silicon, adapted with permission from [74]; (*c*) multiphoton absorption in Gallium Nitride, adapted with permission from [75]; (*d*) intra-band current in Gallium Arsenide, adapted with permission from [76] and (*e*) dynamical Franz–Keldysh effect in Diamond, adapted with permission from [77].

another interpretation, involving the role of core-excitons—bound electron-hole pairs—between the Si 2p states and the CB.

From the previous result, we can anticipate that the ratio between the bandgap energy and the driving photon energy—i.e. the excitation regime—will modify the physics at play. This was strikingly evidenced in [61], in which XTAS was this time applied to pure silicon, a semiconductor with 3.2 eV direct bandgap (figure 4*b*). Here, real carriers are injected into

the conduction band by a strong IR field, yielding a transient absorption at the Si L-edge persisting for approximately 100 fs (not shown here). The VIS-IR photon energy (1.1–2.7 eV) is slightly below the bandgap, implying a nonlinear excitation mechanism. To identify it, the authors focused on the ultrafast build-up of the electronic population, shown in figure 4*b*. A step-wise increase, synchronized with the oscillations of the electric field, is apparent. The Keldysh adiabaticity parameter [79] used in the experiment is $\gamma \sim 0.5$, suggesting that tunnelling dominates the excitation over multiphoton absorption. This is in line with the observed kinetics: at each extremum of the driving field, electrons are allowed to tunnel from the VB to the CB.

For $\gamma > 1$, multiphoton excitation is expected to be the dominant mechanism. Mashiko *et al*. [75] studied this case in gallium nitride (GaN, $E_g = 3.35$ eV, figure 4*c*), using a pump pulse intensity I about 100 times smaller than in the previous experiment. Since the Keldysh parameter scales as $\gamma \sim I^{-1/2}$, the excitation is well into the multiphoton regime. At variance with previous studies where the IAP probed core-to-valence transitions, here it probed transitions from the VB/CB to the continuum. As shown in figure 4*c*, the absorption oscillates at three times the driving frequency, providing clear evidence of three-photon absorption. Interestingly, it corresponds to a frequency of 1.16 PHz, providing the first direct observation of optical driving above 1 petahertz.

Recently, the situation was studied in the case of a slightly lower bandgap material, gallium arsenide (GaAs) [76]. Here, resonant one photon excitation from the VB to the CB is possible, which could suggest a simple monotonic increase of the absorption. On the contrary, Schlaepfer and co-workers measured 2ω-oscillations across both the VB and CB (figure 4*d*) by probing the system from the As 3d core-level. Accompanying simulations separated the dynamics into inter- and intra-band contributions and showed that the intra-band part—the laser-driven motion of electrons inside one band—explains the observation. Not only is this mechanism responsible for the absorption oscillations, but it surprisingly also increases the number of carriers injected into the CB by nearly a factor of three. This brings a new perspective to the omnipresent phenomenon of resonant excitation in semi-conductors.

Lastly, we might wonder what happens in the intermediate situation, where excitation of real carriers is possible but the field is also strong enough to distort the band structure. Lucchini *et al*. [77] answered this question by studying diamond, which has direct and indirect bandgaps of 7.3 and 5.4 eV, respectively. Here, the infrared pulse is strong enough to promote real carriers to the CB by multiphoton transitions, making it difficult to disentangle this effect from band-structure modifications. The authors ingeniously circumvent this issue by using the IAP to probe transitions from the lower VB to the higher CB, where carriers are absent. There, they measured strong 2ω-oscillations, indicative of a dynamical Franz–Keldysh effect [72], in which the electronic wave functions are periodically modified by the laser pulse, leading to oscillations of the XUV absorption.

These results all show the capabilities of XTAS of capturing the response of electrons during their interaction with a strong pulse with sub-cycle time resolution. This technique now constitutes a reliable and intuitive way to disentangle the mechanisms underlying light absorption in a solid. The mechanisms described here, as well as additional solid-state strong-field phenomena, are described in greater length in a recent review by Kruchinin *et al*. [80]. Moreover, as our ability to probe dynamics progresses, so does the possibility of controlling them. Ultrafast control in femtosecond chemistry [81,82] emerged as a result of the growing understanding of electronic dynamics through pump–probe spectroscopy. Likewise, understanding how and on what time scale electrons in the solid-state respond to the slope of an intense electric field is a necessary step towards designing quantum control protocols in solids at petahertz frequencies. In addition, the creation of arbitrary light forms at the sub-cycle scale has developed tremendously in the past years, for example, through optical synthesis [83] or pulse shaping techniques [84,85]. We believe that these advances, combined with the measurement capabilities of XTAS showcased here, will soon translate into exciting research in ultrafast quantum control of solids, as recently evidenced in gases [86].

(b) Beyond the pulse overlap: carriers and structural dynamics

In parallel to research on nonlinear effects another branch of table-top XUV spectroscopy blossomed: the measurement of intrinsic properties of materials. Here, driving fields are kept weak, and the interest shifts towards slightly longer time scales. Consider, for example, the case of a photovoltaic cell: upon absorbing sunlight, electrons are excited across the bandgap of a semi-conductor before being extracted as current in an external circuit. The relevant question is no longer that of the excitation mechanism—a simple one photon absorption—but rather how do electrons lose energy before being extracted, what reduces their lifetime or slows down their mobility. Answering these questions allows in turn to design more efficient light harvesting systems, and the same could be said for instance about materials used in photosynthesis or water splitting.

These questions have been widely studied with visible and infrared spectroscopy techniques. The attosecond time resolution of XTAS is less critical here; indeed, because the excitation mechanism is a one photon absorption, carriers follow the intensity profile of the light pulse instead of its electric field, setting the experiment's time resolution to the driver pulse duration, typically in the 5–100 fs range. Instead, researchers have made use of (1) the XUV wavelength of high-harmonic sources, providing sensitivity to the local chemical environment of atoms and (2) the broadband nature of these sources, allowing to track dynamics across most of the band structure of materials at the same time.

(i) Carrier dynamics in semiconductors

We begin by discussing the results of Zürch *et al*. [87], which exemplify these concepts. Here, XTAS is performed in nanocrystalline germanium thin films, a semiconductor whose alloys show great promise for building efficient solar cells [88] and photonic devices [89]. Carriers are excited across the bandgap, and the change in absorption is followed by an IAP covering the Ge M edge (spin–orbit split into $3d_{3/2}$ and $3d_{5/2}$). The attosecond pulse is broad enough to probe transitions to both the VB and CB, making it possible to track the dynamics of holes and electrons simultaneously (figure 5*a*). Using an iterative procedure, the authors decompose the observed transient absorption into contributions from both spin–orbit core states, as well as isolate carrier-induced and heat-induced band shifts (figure 5*b*) from carrier kinetics (figure 5*c*). A minor contribution from core-level broadening is not shown here. By doing so, they image in real time how photoexcited carriers scatter to different valleys of the band structure providing a direct measurement of the energy redistribution in the solid. Indeed, it is seen in figure 5*d* that after a few hundreds of femtoseconds, electrons have accumulated at specific energies, corresponding here to the X_1, Δ_1 and Γ'_2 CB valleys. This shows that even though XTAS is not a momentum-resolved measurement (contrary to e.g. angularly resolved photoemission spectroscopy), information about high-symmetry points in the Brillouin zone can still be recovered due to their higher density of states. Additionally, the authors study the band-shift component as a function of time and pump pulse intensity—which controls the number of excited carriers—and show that the dynamics are ruled by carrier injections as well as lattice dynamics, which will be described in more detail in the following section.

This example showcases the potential of XTAS of capturing 'all-at-once' fs-to-ps dynamics. Recent work [90] coupled this approach with theoretical predictions in silicon, allowing to uncover the role of carriers, phonons and their scattering, from tens of femtoseconds to 200 picoseconds. Moreover, due to the core-level probing, this technique provides local information about the chemical environment of a specific element. This means that in heterogeneous systems, different elements present in the lattice can be probed independently. This was recently applied in germanium–silicon alloys [91], revealing the presence of additional trap states that inhibit electron-hole recombination. We anticipate that this technique will be used in ternary and quaternary systems, in which probing from the various core-levels of the constituent elements will provide new insights in their respective kinetics. This will especially be crucial in elucidating the dynamics of heterojunction-based devices.

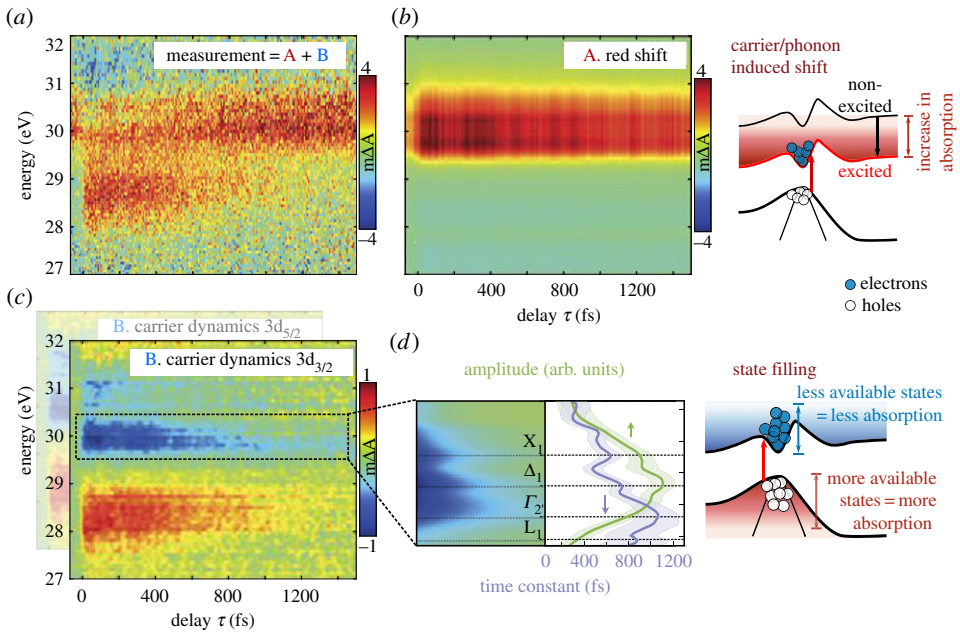

Figure 5. Ultrafast carrier dynamics of Germanium. (*a*) Measured transient absorption trace in nanocrystalline Germanium, which has an indirect gap of 0.66 eV and is probed from the spin–orbit split 3d core-level. The transient trace can be decomposed into two dominating contributions: (*b*) carriers and phonons lead to a redshift of the CB, yielding the positive component shown here. (*c*) When electrons (respectively, holes) are promoted in the CB (respectively, VB), the absorption is reduced (respectively, increased). This leads to the shown transient trace, with the two spin–orbit contributions shifted in energy overlapping in the total trace. (*d*) An exponential fit of each energy slice in the electron dynamics yields time constants corresponding to the lifetimes of carriers at each CB valley, with the longest lifetimes at the low-energy valleys. Adapted with permission from [87].

(ii) Structural dynamics and their interplay with photoexcited carriers

During the relaxation of photoexcited electrons, their energy is redistributed to the crystal lattice. This means that structural dynamics is a key ingredient in understanding and controlling ultrafast electronic dynamics. In solid-state language, structural motion is described as phonons, quasi-particles that are the quantum mechanical description of the elementary vibrations of the lattice. Their role in light–matter interaction is understood as follows: upon absorption of light, energy is first acquired by electrons within the ultrashort pulse duration. Electrons re-establish a Fermi distribution within a few femtoseconds, while the change in the lattice temperature is negligible at this stage. In a second step, electrons interact with phonons through electron–phonon scattering, whereby electrons exchange energy and momentum in order to relax to the conduction band valleys. This energy transfer is rather slow (typically 100 femtoseconds to several picoseconds) due to the much greater mass of phonons compared to electrons, and it is responsible for the long time dynamics in semiconductors previously mentioned in [74,87].

Another possibility is the direct excitation of phonon modes by the pump pulse, one of the prominent mechanisms in the case of non-resonant excitation being impulsive Raman scattering [92]. In the case of an impulsive excitation with a pulse shorter than the period of a phonon, a phonon wave packet is created from the coherent superposition of several phonon states. This leads to coherent vibrations of the lattice, thereby creating modulations in the local electronic environment that XUV absorption is able to probe. Papalazarou *et al*. [93] demonstrated this sensitivity in an early experiment by measuring the transient reflectivity of bismuth with a 39 eV, 10-fs long XUV pulse, whose reflectivity showed oscillations after excitation by a VIS-IR pulse (figure 6*a*) attributed to the A_{1g} phonon mode. More recently, Weisshaupt *et al*. [94] studied

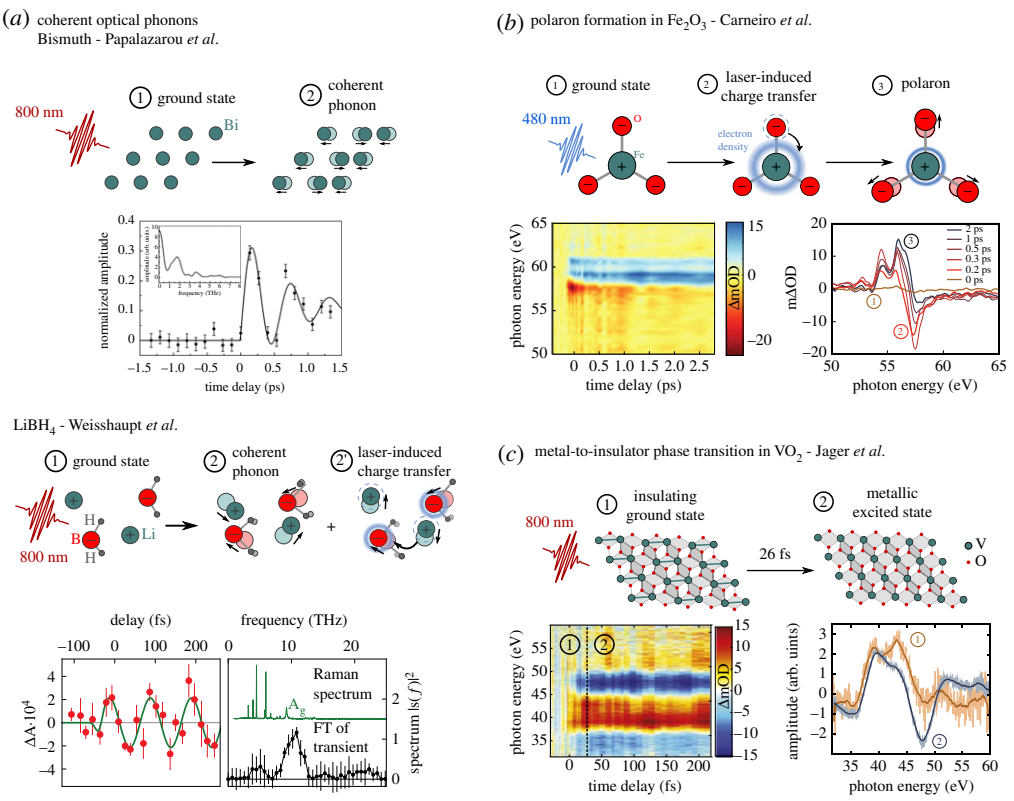

Figure 6. Spectroscopy of coupled electronic and structural dynamics. (*a*) Coherent phonons: Laser excitation can create coherent phonons in Bismuth (top, step 2), leading to oscillations of the XUV reflectivity. Adapted with permission from [93]. The same is true for $LiBH_4$ (bottom, step 2, with atoms shown in the $y = 1/4$ plane of the lattice) but an additional effect appears (step 2′): the laser pulse induces a charge transfer from BH_4^- to Li^+ ions. The resulting polarization also displaces the ions from their equilibrium position. Both displacements are in similar directions, yielding strong oscillations of the XUV absorption (bottom). Adapted with permission from [94]. (*b*) Polaron formation: Upon excitation in the visible range, a charge transfer is initiated in Fe_2O_3 (step 2). It then favours the formation of a polaron, with the additional electronic density localized on the Fe atom (step 3). The spectrally resolved transient absorption allows to follow the three steps of this process in real time. Adapted with permission from [95]. (*c*) Phase transition: When struck by a laser pulse, VO_2 transitions from an insulator to a metal (step 1–2). The transient absorption spectrum gives access to the time scale of this ultrafast process, here measured to be 26 ± 6 fs. At the bottom right are shown lineouts of the absorption for the insulating (1) and metal phase (2). Adapted with permission from [96].

the case of crystalline lithium borohydride ($LiBH_4$), shown in figure 6*b*. Here, both the pump pulse and the pulse driving the harmonic generation are 50 fs long, the resulting limited XUV spectral coverage being improved by a two-colour driving field, as previously explained. The XUV differential absorbance, shown in figure 6*b* for a selected energy, shows clear oscillations at a frequency of 10 THz, corresponding to the frequency of the A_{1g} phonon. Interestingly, here the pump pulse has another effect than driving phonon modes: it directly drives electronic charge transfer from the BH_4^- anion to the Li^+ cation [97] as illustrated by the step 2′ in figure 6*b*. This creates a transient dipole across the bond and a force that displaces the nuclei from their equilibrium positions. The authors show that this force overlaps strongly with the A_{1g} phonon mode, enhancing its excitation through an interplay of electronic and structural dynamics.

This interplay between electronic and nuclear dynamics manifests itself in condensed matter in numerous ways. Consider now the structure of haematite (α-Fe_2O_3), depicted in figure 6*c*, in

which a similar mechanism takes place: upon photoexcitation, electron density is shifted from the O to the Fe atom [98]. This charge transfer is of central importance in several applications: due to its bandgap of 2 eV and its abundance on Earth, Fe_2O_3 is a strong candidate for solar water splitting and artificial photosynthesis [99]. However, it has been observed that photoexcited carriers recombine in picoseconds and show poor mobility, precluding its use in efficient devices. Carneiro *et al*. [95] tackled this bottleneck using XTAS and showed that at the root of this short lifetime is an electron–phonon coupling. Indeed, once the charge transfer has taken place, a dipole is created between the neighbouring ions, inducing a shift of their position. In this specific case, this effect is strong enough to form a polaron—a quasi-particle constituted by an electron and a microscopic polarization, depicted as step 3 in figure 6*c*. Owing to the charge-induced nuclear motion, the electronic wave function is strongly localized on the Fe centre, drastically limiting the carrier mobility: electrons can then only travel via phonon-mediated hops between iron centres. In the experiment of Carneiro *et al*., the charge transfer step and the polaron formation are subsequently observed, and the process is studied as a function of photoexcitation wavelength. This provides unique insight into the photoconversion processes of this material and explains the underwhelming efficiency of current devices. Subsequent studies explored this phenomenon even further and showcased the role of structure and bonding [89] as well as surface trapping [90] in polaron formation.

Finally, electronic and structural effects can lead to even more drastic changes: in the so-called strongly correlated materials, small perturbations are able to tip the system from one phase to another. A canonical example is VO_2, which undergoes an insulator-to-metal transition at 340 K, in which its crystal structure quickly changes from monoclinic to rutile (figure 6*d*). The underlying mechanism has long been debated: is it due to a structural instability (a Peierls transition, similar to a dimerization [100]), or an effect purely driven by electron correlations (a Mott–Hubard transition [101,102]), or a combination of both? XTAS presents us with a way to answer this question: if the phase transition is initiated by a laser pulse, the subsequent electronic and structural dynamics can be observed from the first few femtoseconds to many picoseconds using an attosecond probe pulse. Jager *et al*. [96] used this approach to measure a 26 ± 6 fs transition time between insulating and metallic phases, which, contrary to recent photoemission [102] and optical reflectivity [103] measurements, is not limited by the 6 fs instrument response duration. This time scale excludes purely phonon-driven mechanisms on the basis that the material's phonon mode periods are longer than the observed dynamics; for instance, the V-V dimer stretch, hypothesized to play a role in the transition, has a period of 98 fs. On the other hand, it is not purely due to electronic correlation effects either, whose time scale is given by the plasma frequency, which would be about 4 fs in this study. The answer might involve cooperative electronic and structural effects, which will require accurate modelling of the mapping between electronic screening and structural distortions onto the XUV spectrum.

(iii) Attosecond transient reflectivity spectroscopy

The studies presented here offer physical insight into relevant problems in condensed matter. However, XTAS is still a developing field and is currently performed in a limited set of specialized laboratories around the world. Here we provide our perspective on the current state of the field and in which the direction of current efforts are going, in order to make the technique generally applicable to most topics of condensed matter.

One of the most active fields in solid-state physics is the study of quantum matter. Although its definition is slightly fuzzy—after all, all matter is quantum at some level—it generally comprises states of matter where macroscopic properties emerge from intrinsically quantum mechanical effects. These materials show highly unusual features such as non-trivial topological properties (e.g. topological insulators, Weyl semimetals) or superconductivity. Beyond its fundamental interest, quantum matter is actively researched to be integrated into devices: transistors, light harvesting, quantum computing, catalysis, which could be improved by using these materials. Creating and manipulating such materials can however be a challenge in itself; which brings

us to perhaps a significant limitation of XTAS for solid-state spectroscopy: the limited number of systems that can be studied in well-ordered thin films. Indeed, not all materials can be synthetized in films thin enough to transmit XUV light, of the order of 10 s to 100 s of nm, and their properties sometimes only emerge in the case of clean, single-crystalline samples. In addition, thin films conduct heat poorly, oftentimes to the extent that their temperature does not have time to relax between each laser pulse. This leads to unwanted persistent contributions in their absorption such as heat-induced band shifts [87]. Finally, XTAS is blind to the surface properties of matter, preventing the study of the chemistry of interfaces.

A way to overcome these limitations is to instead perform transient reflectivity measurements. Aside from an aforementioned early work [93], this technique has very seldom been implemented. It is indeed more technically challenging, due to the reduction of an already scarce XUV flux at the reflection interface and more difficult experimental implementation. Additionally, the reflectivity of a sample is governed by the Fresnel equations, combining imaginary and real parts of the dielectric function, and it depends on the angle of incidence. Disentangling these contributions requires measurements of the reflectivity as a function of polarization or angle, or approximations relying on Kramers–Kronig relations [104]. The past year, however, has seen the emergence of a few experiments using this technique. Cirri *et al*. [105] combined both XUV transient absorption and reflectivity to investigate single crystals of several transition metal oxides and demonstrated that only 3 nm were probed in reflection geometry—a surface sensitivity similar to photoemission spectroscopy. Kaplan *et al*. [106] demonstrated that the relaxation of both holes and electrons in crystalline germanium could be tracked by XUV transient reflectivity. Finally, the electronic dynamics of Fe_2O_3 were revisited in reflectivity [107,108], evidencing the competition between surface electron trapping and polaron formation.

4. Perspectives for attosecond spectroscopy

First, we point out that most of the studies presented in this review (and all of the solid-state experiments) were performed using XUV fields generated by VIS–NIR drivers. The reason is technological; titanium sapphire lasers at 800 nm have been the sources of choice for attosecond science. As was shown by the first gas-phase experiments at the carbon K-edge, higher photon energies can extend XTAS to deeper core-levels of elements. These core-levels are simpler to simulate and understand due to their reduced interaction with valence levels. Moreover, some core-levels dominate the properties of elements; for instance, magnetic properties of transition metals are governed by 3d electronic states and are thus better measured at the L-edge (2p to 3d transitions, at about 700 eV in the case of iron). Finally, accessing the carbon, oxygen and nitrogen K-edges allows the study of biological systems (e.g. nucleotides [109] or amino acids [110,111]), as well as promising materials such as graphene [112]. The main difficulty so far is the low photon flux, which experimentalists have tried to increase by using semi-infinite gas cells [113] or driving the HHG process with a few-cycle NIR pulse [114]. These improvements recently demonstrated the production of IAPs based either on phase matching arguments [115] or amplitude gating [116,117], and complete characterization of these pulses has been performed [118,119].

Two recent studies [113,120] made a decisive advance in extending XTAS further in the X-ray, by performing static absorption measurements of solids in the soft X-ray region across bandwidths of more than 100 eV. This allowed them to measure the so-called absorption fine-structure appearing above absorption edges, which shows oscillations resulting from electronic interferences between neighbouring atoms. Fitting the fine-structure with reconstruction algorithms allows one to recover interatomic distances, which if done in a pump–probe experiment could yield real-time, Ångström-resolved measurements of the lattice structure, with remarkable time resolution. This prospect holds great promise notably to study coupled electronic and structural dynamics underlying phase transitions. Another significant step was achieved by Buades *et al*. [121], who performed attosecond-resolved XTAS measurements in semi-metallic TiS_2 at the Ti L-edge, lying at 460 eV. This constitutes the first solid-state XTAS experiment in the soft X-ray.

Table 1. Examples of experimental techniques generating few-cycle ultraviolet pulses.

technique	spanning wavelength (nm)	driving field	maximum output	duration	tunable?
photonic crystal hollow core fibres [122]	113–1000	1042 nm	$\ll$1 µJ	not recompressed	yes
super continuum achromatic doubling [123]	245–300	visible super continuum	$<$1 µJ	$<$8 fs	yes
four wave mixing in hollow core fibre [124]	260–285	750 + 400 nm	300 nJ	$<$10 fs	no
four wave mixing in laser filamentation [125]	250–270	800 nm + 400 nm	20 µJ	12 fs	no
HHG in gas cell [126,127]	250–280	750 nm continuum	1.2 µJ	$<$4 fs	no

In addition to extending probe wavelengths, novel insight can be gained by improving control of the excitation pulse. Indeed, to study near-equilibrium dynamics before any relaxation occurs it is desirable to design experiments with time resolution faster than the nuclear motion time scale. Molecular hydrogen possesses the fastest ground-state vibrational period of 7 fs, so pulses capable of driving dynamics on this time scale are necessary. Additionally, in numerous molecular systems, HOMO to LUMO transitions are accessible in the mid-ultraviolet range from 200 to 300 nm. Likewise, such wavelengths would allow resonant excitation of solids with larger bandgap. In total, 266 nm is often used as it is the third harmonic of femtosecond Ti : sapphire lasers and the fourth harmonic of nanosecond Nd : Yag lasers, but even at this wavelength the generation of intense few-cycle pulses is challenging. A number of techniques are currently being developed, which we anticipate will be soon implemented in XTAS set-ups. In table 1, we survey a non-exhaustive list of such techniques.

One notable absentee from this review is the question of chirality. So far, the technical bottleneck in accessing either molecular chirality or the magnetism of materials has been the reliable generation of circularly polarized XUV and X-ray light. This has been a long-standing challenge for the attosecond community, which was overcome only recently. New generation techniques, based on multilayer XUV mirrors [127,128], molecular shape resonances [129] and bi-colour driving fields [130–133], were used to generate discrete spectra of elliptically polarized harmonics. Recently, the generation of a circularly polarized IAP was also observed [134]. There is little doubt that these techniques will soon be implemented in XTAS apparatus, as it would allow to simultaneously perform circular dichroism measurements, i.e. the difference in absorption between right and left circularly polarized XUV light. In XTAS, it will be combined with attosecond or few-femtosecond temporal resolution, providing unique insight into ultrafast spin and orbital dynamics. This will shed new light on light-induced demagnetization [135], whose mechanisms are still debated [136], coherent magnetization [137] or magnetization reversal [138], especially for heterogeneous systems. In the case of molecules, it will provide eniantospecific attosecond photodynamics, which are just beginning to be explored [139].

Data accessibility. This article has no additional data.

Authors' contributions. R.G. and H.J.B.M. wrote the manuscript with inputs from all authors.

Competing interests. We declare we have no competing interests.

Funding. H.J.B.M., S.R.L. and D.M.N. acknowledge the Director, Office of Science, Office of Basic Energy Sciences, through the Atomic, Molecular, and Optical Sciences Program and the Gas Phase Chemical Physics Program, of the Division of Chemical Sciences, Geosciences, and Biosciences, and S.R.L. acknowledges the Physical Chemistry of Inorganic Nanostructures Program, KC3103, of the Division of Materials and Engineering, of the US Department of Energy at LBNL under contract no. DE-AC02-05CH11231 for funding. The authors also gratefully acknowledge financial support from the Defense Advanced Research Projects

Agency PULSE Program Grant W31P4Q-13-1-0017, the Army Research Office MURI grant no. W911NF-14-1-0383, and the U.S. Air Force Office of Scientific Research No. FA9550-15-1-0037. A.G. and S.R.L. also acknowledge the National Science Foundation under grant CHE-1660417. A.G. acknowledges support from the German Research Foundation (GU 1642/1-1). S.R.L. and R.G. also acknowledge the AFOSR under grant no. FA9550-14-1-0154. The authors gratefully acknowledge the National Science Foundation for an equipment grant no. MRI-1624322. S.R.L. acknowledges the support of an AFOSR DURIP grant no. FA9550-16-1-0281.
Acknowledgements. The authors acknowledge Lou Barreau for fruitful discussions.

References

1. Röntgen WC. 1898 Über eine neue Art von Strahlen. *Ann. Phys.* **300**, 12–17.
2. Zhong J, Zhang H, Sun X, Lee ST. 2014 Synchrotron soft X-ray absorption spectroscopy study of carbon and silicon nanostructures for energy applications. *Adv. Mater.* **26**, 7786–7806. (doi:10.1002/adma.201304507)
3. Meirer F, Weckhuysen BM. 2018 Spatial and temporal exploration of heterogeneous catalysts with synchrotron radiation. *Nat. Rev. Mater.* **3**, 324–340. (doi:10.1038/s41578-018-0044-5)
4. Beamson G, Briggs D. 1992 High resolution monochromated X-ray photoelectron spectroscopy of organic polymers: a comparison between solid state data for organic polymers and gas phase data for small molecules. *Mol. Phys.* **76**, 919–936. (doi:10.1080/00268979200101761)
5. Schofield EJ. 2018 Illuminating the past: X-ray analysis of our cultural heritage. *Nat. Rev. Mater.* **3**, 285–287. (doi:10.1038/s41578-018-0037-4)
6. Munro IH, Schwentner N. 1983 Time resolved spectroscopy using synchrotron radiation. *Nucl. Instruments Methods Phys. Res.* **208**, 819–834. (doi:10.1016/0167-5087(83)91227-9)
7. Zewail AH. 2000 Femtochemistry: atomic-scale dynamics of the chemical bond using ultrafast lasers (Nobel lecture). *Angew. Chemie - Int. Ed.* **39**, 2586–2631. (doi:10.1002/1521-3773(20000804)39:15<2586::AID-ANIE2586>3.0.CO;2-O)
8. McNeil BWJ, Thompson NR. 2010 X-ray free-electron lasers. *Nat. Photonics* **4**, 814–821. (doi:10.1038/nphoton.2010.239)
9. Zhao Z, Wang D, Gu Q, Yin L, Gu M, Leng Y, Liu B. 2017 Status of the SXFEL facility. *Appl. Sci.* **7**, 607. (doi:10.3390/app7060607)
10. Pellegrini C, Marinelli A, Reiche S. 2016 The physics of X-ray free-electron lasers. *Rev. Mod. Phys.* **88**, 15006. (doi:10.1103/RevModPhys.88.015006)
11. Seddon EA *et al.* 2017 Short-wavelength free-electron laser sources and science: a review. *Reports Prog. Phys.* **80**, 115901. (doi:10.1088/1361-6633/aa7cca)
12. Zholents A, Zolotorev M. 1996 Femtosecond X-ray pulses of synchrotron radiation. *Phys. Rev. Lett.* **76**, 912–915. (doi:10.1103/PhysRevLett.76.912)
13. Schoenlein RW. 2000 Generation of femtosecond pulses of synchrotron radiation. *Science* **287**, 2237–2240. (doi:10.1126/science.287.5461.2237)
14. McPherson A, Gibson G, Jara H, Johann U, Luk TS, McIntyre IA, Boyer K, Rhodes CK. 1987 Studies of multiphoton production of vacuum-ultraviolet radiation in the rare gases. *J. Opt. Soc. Amer. B* **4**, 595–601. (doi:10.1364/JOSAB.4.000595)
15. Ferray M, l'Huillier A, Li XF, Lompre LA, Mainfray G, Manus C. 1988 Multiple-harmonic conversion of 1064 nm radiation in rare gases. *J. Phys. B At. Mol. Opt. Phys.* **21**, L31–L35. (doi:10.1088/0953-4075/21/3/001)
16. Chini M *et al.* 2014 Coherent phase-matched VUV generation by field-controlled bound states. *Nat. Photonics* **8**, 437–441. (doi:10.1038/nphoton.2014.83)
17. Calegari F, Sansone G, Stagira S, Vozzi C, Nisoli M. 2016 Advances in attosecond science. *J. Phys. B-Atomic Mol. Opt. Phys.* **49**, 062001. (doi:10.1088/0953-4075/49/6/062001)
18. Boutu W, Ducousso M, Hergott J-F, Merdji H. 2015 Overview on HHG high-flux sources. In *Optical technologies for extreme-ultraviolet and soft X-ray coherent sources* (eds F Canova, L Poletto), pp. 63–78. Berlin, Germany: Springer.
19. Krausz F, Ivanov M. 2009 Attosecond physics. *Rev. Mod. Phys.* **81**, 163. (doi:10.1103/RevModPhys.81.163)
20. Corkum PB, Krausz F. 2007 Attosecond science. *Nat. Phys.* **3**, 381–387. (doi:10.1038/nphys620)

21. Ramasesha K, Leone SR, Neumark DM. 2016 Real-time probing of electron dynamics using attosecond time-resolved spectroscopy. *Annu. Rev. Phys. Chem.* **67**, 61–63. (doi:10.1146/annurev-physchem-040215-112025)
22. Pfeifer T, Spielmann C, Gerber G. 2006 Femtosecond x-ray science. *Reports Prog. Phys.* **69**, 443. (doi:10.1088/0034-4885/69/2/R04)
23. Kraus PM, Zürch M, Cushing SK, Neumark DM, Leone SR. 2018 The ultrafast X-ray spectroscopic revolution in chemical dynamics. *Nat. Rev. Chem.* **2**, 82–94. (doi:10.1038/s41570-018-0008-8)
24. Pollard WT, Mathies RA. 1992 Analysis of femtosecond dynamic absorption spectra of nonstationary states. *Annu. Rev. Phys. Chem.* **43**, 497–523. (doi:10.1146/annurev.pc.43.100192.002433)
25. Bucksbaum PH, Zavriyev A, Muller HG, Schumacher DW. 1990 Softening of the H_2^+ molecular bond in intense laser fields. *Phys. Rev. Lett.* **64**, 1883–1886. (doi:10.1103/PhysRevLett.64.1883)
26. Zavriyev A, Bucksbaum PH, Squier J, Saline F. 1993 Light-induced vibrational structure in H_2^+ and D_2^+ in intense laser fields. *Phys. Rev. Lett.* **70**, 1077–1080. (doi:10.1103/PhysRevLett.70.1077)
27. Kau LS, Spira-Solomon DJ, Penner-Hahn JE, Hodgson KO, Solomon EI. 1987 X-ray absorption edge determination of the oxidation state and coordination number of copper: application to the Type 3 Site in Rhus vernicifera Laccase and its reaction with oxygen. *J. Am. Chem. Soc.* **109**, 6433–6442. (doi:10.1021/ja00255a032)
28. Westre TE, Kennepohl P, DeWitt JG, Hedman B, Hodgson KO, Solomon EI. 1997 A multiplet analysis of Fe K-edge 1 $\rightarrow$ 3d pre-Edge features of iron complexes. *J. Am. Chem. Soc.* **119**, 6297–6314. (doi:10.1021/ja964352a)
29. Kulander KC, Schafer KJ, Krause JL. 1992 Time-dependent studies of multiphoton processes. In *Atoms in intense laser fields* (ed. M Gavrila), p. 247.
30. Corkum PB. 1993 Plasma perspective on strong-field multiphoton ionization. *Phys. Rev. Lett.* **71**, 1994–1997. (doi:10.1103/PhysRevLett.71.1994)
31. Yanai T, Kurashige Y, Mizukami W, Chalupský J, Lan TN, Saitow M. 2015 Density matrix renormalization group for ab initio calculations and associated dynamic correlation methods: a review of theory and applications. *Int. J. Quantum Chem.* **115**, 283–299. (doi:10.1002/qua.24808)
32. Curchod BFE, Martínez TJ. 2018 Ab initio nonadiabatic quantum molecular dynamics. *Chem. Rev.* **118**, 3305–3336. (doi:10.1021/acs.chemrev.7b00423)
33. Perry MD, Crane JK. 1993 High-order harmonic emission from mixed fields. *Phys. Rev. A* **48**, R4051–R4054. (doi:10.1103/PhysRevA.48.R4051)
34. Attar AR, Piticco L, Leone SR. 2014 Core-to-valence spectroscopic detection of the CH2Br radical and element-specific femtosecond photodissociation dynamics of CH2IBr. *J. Chem. Phys.* **141**, 164308. (doi:10.1063/1.4898375)
35. Attar AR, Bhattacherjee A, Leone SR. 2015 Direct observation of the transition-state region in the photodissociation of CH3I by femtosecond extreme ultraviolet transient absorption spectroscopy. *J. Phys. Chem. Lett.* **6**, 5072–5077. (doi:10.1021/acs.jpclett.5b02489)
36. Ryland ES, Lin MF, Verkamp MA, Zhang KL, Benke K, Carlson M, Vura-Weis J. 2018 Tabletop femtosecond M-edge X-ray absorption near-edge structure of FeTPPCI: metalloporphyrin photophysics from the perspective of the metal. *J. Am. Chem. Soc.* **140**, 4691–4696. (doi:10.1021/jacs.8b01101)
37. Bhattacherjee A, Das Pennaraju C, Schnorr K, Attar AR, Leone SR. 2017 Ultrafast intersystem crossing in acetylacetone via femtosecond X-ray transient absorption at the carbon K-edge. *J. Am. Chem. Soc.* **139**, 16 576–16 583. (doi:10.1021/jacs.7b07532)
38. Bhattacherjee A, Attar AR, Leone SR. 2016 Transition state region in the A-Band photodissociation of allyl iodide-A femtosecond extreme ultraviolet transient absorption study. *J. Chem. Phys.* **144**, 124311. (doi:10.1063/1.4944930)
39. Drescher L, Galbraith MCE, Reitsma G, Dura J, Zhavoronkov N, Patchkovskii S, Vrakking MJJ, Mikosch J. 2016 Communication: XUV transient absorption spectroscopy of iodomethane and iodobenzene photodissociation. *J. Chem. Phys.* **145**, 011101. (doi:10.1063/1.4955212)

40. Rury AS, Sension RJ. 2013 Broadband ultrafast transient absorption of iron (III) tetraphenylporphyrin chloride in the condensed phase. *Chem. Phys.* **422**, 220–228. (doi:10.1016/j.chemphys.2013.01.025)
41. Zhang KL, Lin MF, Ryland ES, Verkamp MA, Benke K, de Groot FMF, Girolami GS, Vura-Weis J. 2016 Shrinking the synchrotron: tabletop extreme ultraviolet absorption of transition-metal complexes. *J. Phys. Chem. Lett.* **7**, 3383–3387. (doi:10.1021/acs.jpclett.6b01393)
42. Popmintchev T *et al.* 2012 Bright coherent ultrahigh harmonics in the keV X-ray regime from mid-infrared femtosecond lasers. *Science* **336**, 1287–1291. (doi:10.1126/science.1218497)
43. Attar AR, Bhattacherjee A, Pemmaraju CD, Schnorr K, Closser KD, Prendergast D, Leone SR. 2017 Femtosecond x-ray spectroscopy of an electrocyclic ring-opening reaction. *Science* **356**, 54–59. (doi:10.1126/science.aaj2198)
44. Pertot Y *et al.* 2017 Time-resolved x-ray absorption spectroscopy with a water window high-harmonic source. *Science* **355**, 264–267. (doi:10.1126/science.aah6114)
45. Chini M, Zhao K, Chang ZH. 2014 The generation, characterization and applications of broadband isolated attosecond pulses. *Nat. Photonics* **8**, 178–186. (doi:10.1038/nphoton.2013.362)
46. Goulielmakis E *et al.* 2010 Real-time observation of valence electron motion. *Nature* **466**, 739–743. (doi:10.1038/nature09212)
47. Kobayashi Y, Reduzzi M, Chang KF, Timmers H, Neumark DM, Leone SR. 2018 Selectivity of electronic coherence and attosecond ionization delays in strong-field double ionization. *Phys. Rev. Lett.* **120**, ARTN 2332011. (doi:10.1103/PhysRevLett.120.233201)
48. Wei ZR, Li JL, Wang L, See ST, Jhon MH, Zhang YF, Shi F, Yang MH, Loh ZH. 2017 Elucidating the origins of multimode vibrational coherences of polyatomic molecules induced by intense laser fields. *Nat. Commun.* **8**, ARTN 735. (doi:10.1038/s41467-017-00848-2)
49. Ott C, Kaldun A, Raith P, Meyer K, Laux M, Evers J, Keitel CH, Greene CH, Pfeifer T. 2013 Lorentz meets fano in spectral line shapes: a universal phase and its laser control. *Science* **340**, 716–720. (doi:10.1126/science.1234407)
50. Kaldun A *et al.* 2016 Observing the ultrafast buildup of a Fano resonance in the time domain. *Science* **354**, 738–741. (doi:10.1126/science.aah6972)
51. Lefebvre-Brion H, Field RW. 2004 *The spectra and dynamics of diatomic molecules*. Amsterdam, The Netherlands: Elsevier.
52. Gaarde MB, Buth C, Tate JL, Schafer KJ. 2011 Transient absorption and reshaping of ultrafast XUV light by laser-dressed helium. *Phys. Rev. A* **83**, 013419. (doi:10.1103/PhysRevA.83.013419)
53. Hamm P, Zanni M. 2011 *Concepts and methods of 2D infrared spectroscopy*. Cambridge, UK: Cambridge University Press.
54. Osley EJ, Biris CG, Thompson PG, Jahromi RRF, Warburton PA, Panoiu NC. 2013 Fano resonance resulting from a tunable interaction between molecular vibrational modes and a double continuum of a plasmonic metamolecule. *Phys. Rev. Lett.* **110**, 087402. (doi:10.1103/PhysRevLett.110.087402)
55. Gruson V *et al.* 2016 Attosecond dynamics through a Fano resonance: monitoring the birth of a photoelectron. *Science* **354**, 734–738. (doi:10.1126/science.aah5188)
56. Mukamel S. 1995 *Principles of nonlinear optical spectroscopy*. Oxford, UK: Oxford University Press.
57. Cao W, Warrick ER, Fidler A, Leone SR, Neumark DM. 2016 Near-resonant four-wave mixing of attosecond extreme-ultraviolet pulses with near-infrared pulses in neon: detection of electronic coherences. *Phys. Rev. A* **94**, ARTN 021802. (doi:10.1103/PhysRevA.94.021802)
58. Cao W, Warrick ER, Fidler A, Neumark DM, Leone SR. 2016 Noncollinear wave mixing of attosecond XUV and few-cycle optical laser pulses in gas-phase atoms: Toward multidimensional spectroscopy involving XUV excitations. *Phys. Rev. A* **94**, ARTN 053846. (doi:10.1103/PhysRevA.94.053846)
59. Bengtsson S *et al.* 2017 Space-time control of free induction decay in the extreme ultraviolet. *Nat. Photonics* **11**, 252–258. (doi:10.1038/nphoton.2017.30)
60. Ding T *et al.* 2016 Time-resolved four-wave-mixing spectroscopy for inner-valence transitions. *Opt. Lett.* **41**, 709–712. (doi:10.1364/OL.41.000709)

61. Cao W, Warrick ER, Fidler A, Leone SR, Neumark DM. 2018 Excited-state vibronic wave-packet dynamics in H_2 probed by XUV transient four-wave mixing. *Phys. Rev. A* **97**, 23401. (doi:10.1103/PhysRevA.97.023401)
62. Warrick ER, Fidler A, Cao W, Bloch E, Neumark DM, Leone SR. 2018 Multiple pulse coherent dynamics and wave packet control of the N_2 a′ 1 Σ_g^+ dark state by attosecond four wave mixing. *Faraday Discuss.* **212**, 157–174. (doi:10.1039/C8FD00074C)
63. Marroux HJB, Fidler AP, Neumark DM, Leone SR. 2018 Multidimensional spectroscopy with attosecond extreme ultraviolet and shaped near-infrared pulses. *Sci. Adv.* **4**, eaau3783. (doi:10.1126/sciadv.aau3783)
64. Drude P. 1900 Zur Elektronentheorie der Metalle; II. Teil. Galvanomagnetische und thermomagnetische Effecte. *Ann. Phys.* **308**, 369–402. (doi:10.1002/andp.19003081102)
65. Sommerfeld A, Bethe H. 1933 Elektronentheorie der Metalle. In *Aufbau Der zusammenhängenden materie*.
66. Bloch F. 1929 Uber die Quantenmechanik der Elekronen in Kristallgittern. *Zeitschrift für Phys. A* **52**, 555–600. (doi:10.1007/BF01339455)
67. Kittel C. 1963 *Quantum theory of solids*. New York, NY: Wiley.
68. Zener C. 1934 A theory of the electrical breakdown of solid dielectrics. *Proc. R. Soc. Lond. A* **145**, 523–529. (doi:10.1098/rspa.1934.0116)
69. Kane EO. 1960 Zener tunneling in semiconductors. *J. Phys. Chem. Solids* **12**, 181–188. (doi:10.1016/0022-3697(60)90035-4)
70. Emin D, Hart CF. 1987 Existence of Wannier-Stark localization. *Phys. Rev. B* **36**, 7353–7359. (doi:10.1103/PhysRevB.36.7353)
71. Wannier GH. 1959 *Elements of Solid State Theory*.
72. Jauho AP, Johnsen K. 1996 Dynamical Franz-Keldysh effect. *Phys. Rev. Lett.* **76**, 4576. (doi:10.1103/PhysRevLett.76.4576)
73. Schultze M *et al.* 2013 Controlling dielectrics with the electric field of light. *Nature* **493**, 75–78. (doi:10.1038/nature11720)
74. Schultze M *et al.* 2014 Attosecond band-gap dynamics in silicon. *Science* **346**, 1348–1352. (doi:10.1126/science.1260311)
75. Mashiko H, Oguri K, Yamaguchi T, Suda A, Gotoh H. 2016 Petahertz optical drive with wide-bandgap semiconductor. *Nat. Phys.* **12**, 741–745. (doi:10.1038/nphys3711)
76. Schlaepfer F, Lucchini M, Sato SA, Volkov M, Kasmi L, Hartmann N, Rubio A, Gallmann L, Keller U. 2018 Attosecond optical-field-enhanced carrier injection into the GaAs conduction band. *Nat. Phys.* **14**, 560–564. (doi:10.1038/s41567-018-0069-0)
77. Lucchini M *et al.* 2016 Attosecond dynamical Franz-Keldysh effect in polycrystalline diamond. *Science* **353**, 916–919. (doi:10.1126/science.aag1268)
78. Moulet A, Bertrand JB, Klostermann T, Guggenmos A, Karpowicz N, Goulielmakis E. 2017 Soft x-ray excitonics. *Science* **357**, 1134–1138. (doi:10.1126/science.aan4737)
79. Keldysh LV. 1964 Ionization in the field of a strong electromagnetic wave. *Zh. Eksperim. i Teor. Fiz.* **47**, 1307–1314.
80. Kruchinin SY, Krausz F, Yakovlev VS. 2018 ColloquiumâĂŕ: strong-field phenomena in periodic systems. *Rev. Mod. Phys.* **90**, 021002. (doi:10.1103/RevModPhys.90.021002)
81. Zewail AH. 1994 *Femtochemistry: ultrafast dynamics of the chemical bond*. Singapore: World Scientific Publishing Company.
82. Shapiro M, Brumer P. 2003 *Principles of the quantum control of molecular processes*. Hoboken, NJ: Wiley-Interscience.
83. Hassan MT *et al.* 2016 Optical attosecond pulses and tracking the nonlinear response of bound electrons. *Nature* **530**, 66. (doi:10.1038/nature16528)
84. Weiner AM, Leaird DE, Patel JS, Wullert JR. 1990 Programmable femtosecond pulse shaping by use of a multielement liquid-crystal phase modulator. *Opt. Lett.* **15**, 326–328. (doi:10.1364/OL.15.000326)
85. Kaindl RA, Wurm M, Reimann K, Hamm P, Weiner AM, Woerner M. 2000 Generation, shaping, and characterization of intense femtosecond pulses tunable from 3 to 20 μm. *J. Opt. Soc. Am. B* **17**, 2086–2094. (doi:10.1364/JOSAB.17.002086)
86. Hütten K *et al.* 2018 Ultrafast quantum control of ionization dynamics in krypton. *Nat. Commun.* **9**, 719. (doi:10.1038/s41467-018-03122-1)

87. Zürch M *et al.* 2017 Direct and simultaneous observation of ultrafast electron and hole dynamics in germanium. *Nat. Commun.* **8**, 15734. (doi:10.1038/ncomms15734)
88. King RR, Law DC, Edmondson KM, Fetzer CM, Kinsey GS, Yoon H, Sherif RA, Karam NH. 2007 40% efficient metamorphic GaInPGaInAsGe multijunction solar cells. *Appl. Phys. Lett.* **90**, 183516. (doi:10.1063/1.2734507)
89. Wirths S *et al.* 2015 Lasing in direct-bandgap GeSn alloy grown on Si. *Nat. Photonics* **9**, 88. (doi:10.1038/nphoton.2014.321)
90. Cushing SK, Zürch M, Kraus PM, Carneiro LM, Lee A, Chang H-T, Kaplan CJ, Leone SR. 2017 Valley-specific hot phonon and carrier relaxation pathways in Si(100) determined by transient extreme ultraviolet spectroscopy. (http://arxiv .org/abs/1705.04393)
91. Zürch M *et al.* 2017 Ultrafast carrier thermalization and trapping in silicon-germanium alloy probed by extreme ultraviolet transient absorption spectroscopy. *Struct. Dyn.* **4**, 044029. (doi:10.1063/1.4985056)
92. Yan YX, Gamble EB, Nelson KA. 1985 Impulsive stimulated scattering: general importance in femtosecond laser pulse interactions with matter, and spectroscopic applications. *J. Chem. Phys.* **83**, 5391–5399. (doi:10.1063/1.449708)
93. Papalazarou E *et al.* 2008 Probing coherently excited optical phonons by extreme ultraviolet radiation with femtosecond time resolution. *Appl. Phys. Lett.* **93**, 041114. (doi:10.1063/1.2966180)
94. Weisshaupt J, Rouzée A, Woerner M, Vrakking MJJ, Elsaesser T, Shirley EL, Borgschulte A. 2017 Ultrafast modulation of electronic structure by coherent phonon excitations. *Phys. Rev. B* **95**, 081101. (doi:10.1103/PhysRevB.95.081101)
95. Carneiro LM, Cushing SK, Liu C, Su Y, Yang P, Alivisatos AP, Leone SR. 2017 Excitation-wavelength-dependent small polaron trapping of photoexcited carriers in α-Fe_2O_3. *Nat. Mater.* **16**, 819–825. (doi:10.1038/nmat4936)
96. Jager MF, Ott C, Kraus PM, Kaplan CJ, Pouse W, Marvel RE, Haglund RF, Neumark DM, Leone SR. 2017 Tracking the insulator-to-metal phase transition in VO_2 with few-femtosecond extreme UV transient absorption spectroscopy *Proc. Natl Acad. Sci. USA* **114**, 9558–9563. (doi:10.1073/pnas.1707602114)
97. Stingl J, Zamponi F, Freyer B, Woerner M, Elsaesser T, Borgschulte A. 2012 Electron transfer in a virtual quantum state of LiBH 4 induced by strong optical fields and mapped by femtosecond X-ray diffraction. *Phys. Rev. Lett.* **109**, 147402. (doi:10.1103/PhysRevLett.109.147402)
98. Vura-Weis J, Jiang CM, Liu C, Gao H, Lucas JM, De Groot FMF, Yang P, Alivisatos AP, Leone SR. 2013 Femtosecond M2,3-edge spectroscopy of transition-metal oxides: photoinduced oxidation state change in α-Fe_2O_3. *J. Phys. Chem. Lett.* **4**, 3667–3671. (doi:10.1021/jz401997d)
99. Lin Y, Yuan G, Sheehan S, Zhou S, Wang D. 2011 Hematite-based solar water splitting: challenges and opportunities. *Energy Environ. Sci.* **4**, 4862. (doi:10.1039/c1ee01850g)
100. Fowler M. 2003 Electrons in one dimensionâĂŤ: the Peierls transition.
101. Imada M, Fujimori A, Tokura Y. 1998 Metal-insulator transitions. *Rev. Mod. Phys.* **70**, 1039–1263. (doi:10.1103/RevModPhys.70.1039)
102. Wegkamp D *et al.* 2014 Instantaneous band gap collapse in photoexcited monoclinic VO_2 due to photocarrier doping. *Phys. Rev. Lett.* **113**, 216401. (doi:10.1103/PhysRevLett.113.216401)
103. O'Callahan BT, Jones AC, Hyung Park J, Cobden DH, Atkin JM, Raschke MB. 2015 Inhomogeneity of the ultrafast insulator-to-metal transition dynamics of VO_2. *Nat. Commun.* **6**, 6849. (doi:10.1038/ncomms7849)
104. Jackson JD. 1999 *Classical electrodynamics*, 3rd edn. New York, NY: John Wiley Sons.
105. Cirri A, Husek J, Biswas S, Baker LR. 2017 Achieving surface sensitivity in ultrafast XUV spectroscopy: M 2,3 edge reflection–absorption of transition metal oxides. *J. Phys. Chem. C* **121**, 15 861–15 869. (doi:10.1021/acs.jpcc.7b05127)
106. Kaplan CJ *et al.* 2018 Femtosecond tracking of carrier relaxation in germanium with extreme ultraviolet transient reflectivity. *Phys. Rev. B* **97**, 205202. (doi:10.1103/PhysRevB.97.205202)
107. Porter IJ, Cushing SK, Carneiro LM, Lee A, Ondry JC, Dahl JC, Chang H-T, Alivisatos AP, Leone SR. 2018 Photoexcited small polaron formation in goethite (α-FeOOH) nanorods probed by transient extreme ultraviolet spectroscopy. *J. Phys. Chem. Lett.* **9**, 4120–4124. (doi:10.1021/acs.jpclett.8b01525)

108. Biswas S, Husek J, Baker LR. 2018 Elucidating ultrafast electron dynamics at surfaces using extreme ultraviolet (XUV) reflection–absorption spectroscopy. *Chem. Commun.* **54**, 4216–4230. (doi:10.1039/C8CC01745J)
109. Wolf TJA *et al.* 2017 Probing ultrafast $\pi\pi_*/n\pi_*$ internal conversion in organic chromophores via K-edge resonant absorption. *Nat. Commun.* **8**, 29. (doi:10.1038/s41467-017-00069-7)
110. Calegari F *et al.* 2014 Ultrafast electron dynamics in phenylalanine initiated by attosecond pulses. *Science* **346**, 336–339. (doi:10.1126/science.1254061)
111. Lara-Astiaso M *et al.* 2018 Attosecond pump-probe spectroscopy of charge dynamics in tryptophan. *J. Phys. Chem. Lett.* **9**, 4570–4577. (doi:10.1021/acs.jpclett.8b01786)
112. Pacilé D, Papagno M, Rodríguez AF, Grioni M. 2008 Near-edge X-ray absorption fine-structure investigation of graphene. *Phys. Rev. Lett.* **101**, 066806. (doi:10.1103/PhysRevLett.101.066806)
113. Popmintchev D *et al.* 2018 Near- and extended-edge X-ray-absorption fine-structure spectroscopy using ultrafast coherent high-order harmonic supercontinua. *Phys. Rev. Lett.* **120**, 093002. (doi:10.1103/PhysRevLett.120.093002)
114. Johnson AS *et al.* 2018 High-flux soft x-ray harmonic generation from ionization-shaped few-cycle laser pulses. *Sci. Adv.* **4**, eaar3761. (doi:10.1126/sciadv.aar3761)
115. Chen MC *et al.* 2014 Generation of bright isolated attosecond soft X-ray pulses driven by multicycle midinfrared lasers. *Proc. Natl Acad. Sci. USA* **111**, E2361–E2367. (doi:10.1073/pnas.1407421111)
116. Cousin SL, Silva F, Teichmann S, Hemmer M, Buades B, Biegert J. 2014 High-flux table-top soft x-ray source driven by sub-2-cycle, CEP stable, 185-μm 1-kHz pulses for carbon K-edge spectroscopy. *Opt. Lett.* **39**, 5383–5386. (doi:10.1364/OL.39.005383)
117. Li J *et al.* 2017 53-attosecond X-ray pulses reach the carbon K-edge. *Nat. Commun.* **8**, 186. (doi:10.1038/s41467-017-00321-0)
118. Cousin SL, Di Palo N, Buades B, Teichmann SM, Reduzzi M, Devetta M, Kheifets A, Sansone G, Biegert J. 2017 Attosecond streaking in the water window: a new regime of attosecond pulse characterization. *Phys. Rev. X* **7**, ARTN 041030. (doi:10.1103/PhysRevX.7.041030)
119. Gaumnitz T, Jain A, Pertot Y, Huppert M, Jordan I, Ardana-Lamas F, Worner HJ. 2017 Streaking of 43-attosecond soft-X-ray pulses generated by a passively CEP-stable mid-infrared driver. *Opt. Express* **25**, 27506–27518. (doi:10.1364/OE.25.027506)
120. Buades B *et al.* 2018 Dispersive soft x-ray absorption fine-structure spectroscopy in graphite with an attosecond pulse. *Optica* **5**, 502–506. (doi:10.1364/OPTICA.5.000502)
121. Buades B *et al.* 2018 Attosecond-resolved petahertz carrier motion in semi-metallic TiS2. *ArXiv e-prints*.
122. Jiang X, Joly NY, Finger MA, Babic F, Wong GKL, Travers JC, Russell PS. 2015 Deep-ultraviolet to mid-infrared supercontinuum generated in solid-core ZBLAN photonic crystal fibre. *Nat. Photonics* **9**, 133–139. (doi:10.1038/nphoton.2014.320)
123. Prokhorenko VI, Picchiotti A, Maneshi S, Dwayne Miller RJ, Yamanouchi K, Cundiff S, de Vivie-Riedle R, Kuwata-Gonokami M, DiMauro L. 2015 *Broadband electronic Two-dimensional spectroscopy in the deep UV*, pp. 432–435. Cham, Switzerland: Springer International Publishing.
124. Kida Y, Liu J, Teramoto T, Kobayashi T. 2010 Sub-10 fs deep-ultraviolet pulses generated by chirped-pulse four-wave mixing. *Opt. Lett.* **35**, 1807–1809. (doi:10.1364/OL.35.001807)
125. Fuji T, Horio T, Suzuki T. 2007 Generation of 12 fs deep-ultraviolet pulses by four-wave mixing through filamentation in neon gas. *Opt. Lett.* **32**, 2481–2483. (doi:10.1364/OL.32.002481)
126. Graf U, Fiess M, Schultze M, Kienberger R, Krausz F, Goulielmakis E. 2008 Intense few-cycle light pulses in the deep ultraviolet. *Opt. Express* **16**, 18 956–18 963. (doi:10.1364/OE.16.018956)
127. Reiter F *et al.* 2010 Generation of sub-3 fs pulses in the deep ultraviolet. *Opt. Lett.* **35**, 2248–2250. (doi:10.1364/OL.35.002248)
128. Willems F *et al.* 2015 Probing ultrafast spin dynamics with high-harmonic magnetic circular dichroism spectroscopy. *Phys. Rev. B* **92**, 220405. (doi:10.1103/PhysRevB.92.220405)
129. Ferré A *et al.* 2015 A table-top ultrashort light source in the extreme ultraviolet for circular dichroism experiments. *Nat. Photonics* **9**, 93–98. (doi:10.1038/nphoton.2014.314)

130. Eichmann H, Egbert A, Nolte S, Momma C, Wellegehausen B, Becker W, Long S, McIver JK. 1995 Polarization-dependent high-order two-color mixing. *Phys. Rev. A* **51**, R3414–R3417. (doi:10.1103/PhysRevA.51.R3414)
131. Fleischer A, Kfir O, Diskin T, Sidorenko P, Cohen O. 2014 Spin angular momentum and tunable polarization in high-harmonic generation. *Nat. Photonics* **8**, 543–549. (doi:10.1038/nphoton.2014.108)
132. Kfir O *et al.* 2015 Generation of bright phase-matched circularly-polarized extreme ultraviolet high harmonics. *Nat. Photonics* **9**, 99–105. (doi:10.1038/nphoton.2014.293)
133. Lambert G *et al.* 2015 Towards enabling femtosecond helicity-dependent spectroscopy with high-harmonic sources. *Nat. Commun.* **6**, 6167.
134. Huang PC *et al.* 2018 Polarization control of isolated high-harmonic pulses. *Nat. Photonics* **12**, 349. (doi:10.1038/s41566-018-0145-0)
135. Beaurepaire E, Merle JC, Daunois A, Bigot JY. 1996 Ultrafast spin dynamics in ferromagnetic nickel. *Phys. Rev. Lett.* **76**, 4250. (doi:10.1103/PhysRevLett.76.4250)
136. Jal E, López-Flores V, Pontius N, Ferté T, Bergeard N, Boeglin C, Vodungbo B, Lüning J, Jaouen N. 2017 Structural dynamics during laser-induced ultrafast demagnetization. *Phys. Rev. B* **95**, 184422. (doi:10.1103/PhysRevB.95.184422)
137. Bigot JY, Vomir M, Beaurepaire E. 2009 Coherent ultrafast magnetism induced by femtosecond laser pulses. *Nat. Phys.* **5**, 515–520. (doi:10.1038/nphys1285)
138. Stanciu CD, Hansteen F, Kimel AV, Kirilyuk A, Tsukamoto A, Itoh A, Rasing T. 2007 All-optical magnetic recording with circularly polarized light. *Phys. Rev. Lett.* **25**, 047601. (doi:10.1103/PhysRevLett.99.047601)
139. Beaulieu S *et al.* 2017 Attosecond-resolved photoionization of chiral molecules. *Science* **358**, 1288–1294. (doi:10.1126/science.aao5624)